

# Using Shapley Values and Variational Autoencoders to Explain Predictive Models with Dependent Mixed Features

Lars Henry Berge Olsen<sup>\*1</sup>, Ingrid Kristine Glad<sup>1</sup>,  
Martin Jullum<sup>2</sup>, and Kjersti Aas<sup>2</sup>

<sup>1</sup>Department of Mathematics, University of Oslo

<sup>2</sup>Norwegian Computing Center

November 29, 2021

## Abstract

Shapley values are today extensively used as a model-agnostic explanation framework to explain complex predictive machine learning models. Shapley values have desirable theoretical properties and a sound mathematical foundation. Precise Shapley value estimates for dependent data rely on accurate modeling of the dependencies between all feature combinations. In this paper, we use a variational autoencoder with arbitrary conditioning (**VAEAC**) to model all feature dependencies simultaneously. We demonstrate through comprehensive simulation studies that **VAEAC** outperforms the state-of-the-art methods for a wide range of settings for both continuous and mixed dependent features. Finally, we apply **VAEAC** to the Abalone data set from the UCI Machine Learning Repository.

## 1 Introduction

Explainable artificial intelligence (XAI) and interpretable machine learning (IML) have become active research fields in recent years (Adadi and Berrada 2018; Molnar 2019). This is a natural consequence as complex machine learning (ML) models are now applied to solve supervised learning problems in many high-risk areas: cancer prognosis (Kourou et al. 2015), credit scoring (Kvamme et al. 2018), and money laundering detection (Jullum, Løland, et al. 2020). The high prediction accuracy of complex ML models often comes at the expense of model interpretability. As the goal of science is to gain knowledge from the collected data, the use of black-box models hinders the understanding of the underlying relationship between the features and the response, and thereby curtail scientific discovery.

Model explanation frameworks from the XAI field extract the hidden knowledge about the underlying data structure captured by a black-box model, and thereby make the model’s decision-making process transparent. This is crucial for, e.g., medical researchers that apply an ML model to obtain well-performing predictions, but who simultaneously also strive to discover important risk factors. Another driving factor is the *Right to Explanation* legislation in EU’s General Data Protection Regulation (GDPR) (European Commission 2016).

---

<sup>\*</sup>E-mail addresses: lholsten@math.uio.no, glad@math.uio.no, jullum@nr.no, and kjersti@nr.no.

A promising explanation methodology, with a strong mathematical foundation and unique theoretical properties, is *Shapley values*. Within XAI, Shapley values are most commonly used as a *model-agnostic* explanation framework for individual predictions, i.e., *local explanations*. The methodology has also been used to provide *global explanations* (Covert et al. 2020; Giudici and Raffinetti 2021; Owen 2014). Model-agnostic means that the explanation methodology does not rely on model internals, such that the Shapley values can be compared across different ML models trained on the same supervised learning problem. Examples of models are neural networks (Gurney 2018), random forest (Breiman 2001), and XGBoost (T. Chen et al. 2015). Local explanation means that Shapely values do not explain the global model behavior across all data instances, but rather locally for an individual observation. See Molnar (2019) for an overview and details of other explanation frameworks.

Shapley values (Shapley 1953) originated in cooperative game theory, but have been re-introduced as a framework for model explanation by Strumbelj and Kononenko (2010, 2014) and Lundberg, Erion, et al. (2018) and Lundberg and Lee (2017). Originally, Shapley values described a possible solution concept of how to fairly distribute the payout of a game to the players based on their contribution to the overall cooperation/payout. The solution concept is based on several desirable axioms for which Shapley values are the unique solution. When applying Shapley values as an explanation framework, we treat the features as the “players”, the machine learning model as the “game”, and the corresponding prediction as the “payout”. In this framework, the difference between the prediction of a specified individual and the global average prediction is fairly distributed among the associated feature values.

Lundberg and Lee (2017) were a major driving force in the popularization of Shapley values for model explanation with their Python library **SHAP**. In their approach, they implicitly assumed independence between the features, as this partially simplifies the Shapley value estimation. However, the estimation is still fundamentally computationally expensive as the number of terms involved in the Shapley value formula, elaborated in the next section, grows exponentially with the number of features. Furthermore, in observational studies, the features are rarely statistically independent and the **independence** approach can therefore compute incorrect explanations, see for example Aas, Jullum, et al. (2021), Frye et al. (2021), and Merrick and Taly (2020).

Aas, Jullum, et al. (2021) extend the ideas of Lundberg and Lee (2017) and propose three methods for modeling the dependence between the features: the **Gaussian**, **copula**, and **empirical** approaches. The same paper demonstrates through simulation studies that these conditional approaches obtain more precise Shapley value estimates than the **independence** approach for moderate to strong dependence between some or all of the features. Aas, Nagler, et al. (2021) further improve the explanation precision by using non-parametric vine copulas (Joe 1996). Redelmeier et al. (2020) extend the methodology to mixed data by modeling the feature dependencies using conditional inference trees (Hothorn et al. 2006). However, these improvements further increase the computational complexity of Shapley values, as we in addition need to estimate the feature dependencies between all feature combinations. Jullum, Redelmeier, et al. (2021) propose to explain groups of related features instead of individual features to decrease the fundamental computational problem for Shapley values.

The above papers use methods from the statistical community to model the feature dependencies, but machine learning methods can also be applied. Two promising ML methodologies for constructing generative models are *generative adversarial network* (GAN) (Goodfellow, Pouget-Abadie, et al. 2014) and *variational autoencoder* (VAE) (Kingma and Welling 2014; Rezende et al. 2014). Both frameworks consist of neural networks (NNs), but with different model setups. They have been used in a wide variety of generative modeling tasks; human image synthesis (Karras et al. 2020), simulating gravitational lensing for dark

matter research (Mustafa et al. 2019), blending and exploring musical scores (Roberts et al. 2018; Simon et al. 2018), and generating coherent novel sentences (Bowman et al. 2016).

Both frameworks have methods that could potentially be used to estimate Shapley values, namely *generative adversarial imputation nets* (GAIN) (Yoon et al. 2018) and *conditional variational autoencoders* (CVAE) (Sohn et al. 2015), respectively. In this paper, we use the *variational autoencoder with arbitrary conditioning* (VAEAC) by Ivanov et al. (2019), which is a generalization of CVAE. VAEAC models the dependencies between all features simultaneously with a *single* variational autoencoder and it supports mixed data. A relatable method has been briefly discussed by Frye et al. (2021). VAEAC’s single model is a great advantage compared to the methods of Aas, Jullum, et al. (2021), Aas, Nagler, et al. (2021), and Redelmeier et al. (2020), which fit a new model for each feature combination. As the number of feature combinations grows exponentially with the number of features, the VAEAC methodology can reduce the computational burden of Shapley values as a model explanation framework.

The rest of the paper is organized as follows. In Section 2, we introduce the concept of Shapley values in the game-theoretical setting and as a local model-agnostic explanation framework with individual explanations. The variational autoencoder with arbitrary conditioning (VAEAC) is introduced in Section 3, where we also show how its methodology is used to estimate precise Shapley values. In Section 4, we conduct thorough simulation studies to illustrate VAEAC’s excellent performance compared to the state-of-the-art methods of Aas, Jullum, et al. (2021), Lundberg and Lee (2017), and Redelmeier et al. (2020). Then, in Section 5, we use VAEAC to generate Shapley value explanations for the Abalone data set from the UCI Machine Learning Repository (Nash et al. 1994). Section 6 ends the paper with some concluding remarks and potential further work. In the Appendix, we provide full mathematical derivations, implementations details, and additional simulation studies.

## 2 Shapley Values

In this section, we first describe Shapley values in cooperative game theory before we discuss how they can be used for model explanation.

### 2.1 Shapley Values in Cooperative Game Theory

Consider a cooperative game of  $M$  players, indexed by  $j = 1, 2, \dots, M$ , where the players try to maximize a payoff. Let  $\mathcal{M}$  be the set of all players and  $\mathcal{S} \subseteq \mathcal{M}$  be any subset of  $\mathcal{M}$ . Then the Shapley value, developed by Lloyd Shapley (1953), for the  $j$ th player is defined as

$$\phi_j = \sum_{\mathcal{S} \subseteq \mathcal{M} \setminus \{j\}} \frac{|\mathcal{S}|!(M - |\mathcal{S}| - 1)!}{M!} (v(\mathcal{S} \cup \{j\}) - v(\mathcal{S})), \quad (1)$$

where  $v(\mathcal{S})$  is the *contribution function* that maps the subset of players to a real number representing the value of the coalition  $\mathcal{S}$ , while  $|\mathcal{S}|$  is the number of players in the coalition. The number of terms in (1) is  $2^{M-1}$ , hence, the complexity grows exponentially with the number of players  $M$ . In game theory, the Shapley value  $\phi_j$  is the payout the  $j$ th player receives for its efforts in the cooperative game. From (1), we see that the payout is just a weighted sum of the player’s marginal contributions to each coalition  $\mathcal{S}$ . Shapley proved that distributing the total gains of the game in this way is *fair* in the sense that (1) satisfies certain important axioms, which are discussed in more detail in, for example, Hart (1989), Roth (1988), and Shapley (1953).

## 2.2 Shapley Values in Model Explanation

Assume that we are in a supervised learning setting where we want to explain a predictive model  $f(\mathbf{x})$  trained on  $\{\mathbf{x}^{(i)}, y^{(i)}\}_{i=1, \dots, N_{\text{train}}}$ , where  $\mathbf{x}_i$  is an  $M$ -dimensional feature vector,  $y_i$  is a univariate response, and  $N_{\text{train}}$  is the number of training observations.

Shapley values as a model-agnostic explanation framework (Lundberg and Lee 2017; Strumbelj and Kononenko 2010, 2014) enable us to fairly explain the prediction  $\hat{y} = f(\mathbf{x})$  for a specific feature vector  $\mathbf{x} = \mathbf{x}^*$ . The fairness aspect of Shapley values in the model explanation setting is discussed in, for example, Aas, Jullum, et al. (2021), H. Chen et al. (2020), and Fryer et al. (2021).

In the Shapley value framework, the predictive model  $f$  replaces the cooperative game and the  $M$ -dimensional feature vector replaces the  $M$  players. The Shapley value  $\phi_j$  describes the importance of the  $j$ th feature in the prediction  $f(\mathbf{x}^*) = \phi_0 + \sum_{j=1}^M \phi_j$ , where  $\phi_0 = \mathbb{E}[f(\mathbf{x})]$ . That is, the sum of the Shapley values explains the difference between the prediction  $f(\mathbf{x}^*)$  and the global average prediction.

To calculate (1), we need to define an appropriate contribution function  $v(\mathcal{S})$  which should resemble the value of  $f(\mathbf{x})$  when only the features in coalition  $\mathcal{S}$  are known. We use the contribution function proposed by Lundberg and Lee (2017), namely the expected outcome of  $f(\mathbf{x})$  conditioned on that the features in  $\mathcal{S}$  take on the values  $\mathbf{x}_{\mathcal{S}}^*$ . That is,

$$v(\mathcal{S}) = \mathbb{E}[f(\mathbf{x}) | \mathbf{x}_{\mathcal{S}} = \mathbf{x}_{\mathcal{S}}^*] = \mathbb{E}[f(\mathbf{x}_{\bar{\mathcal{S}}}, \mathbf{x}_{\mathcal{S}}) | \mathbf{x}_{\mathcal{S}} = \mathbf{x}_{\mathcal{S}}^*] = \int f(\mathbf{x}_{\bar{\mathcal{S}}}, \mathbf{x}_{\mathcal{S}}^*) p(\mathbf{x}_{\bar{\mathcal{S}}} | \mathbf{x}_{\mathcal{S}} = \mathbf{x}_{\mathcal{S}}^*) d\mathbf{x}_{\bar{\mathcal{S}}}, \quad (2)$$

where  $\mathbf{x}_{\mathcal{S}} = \{x_j : j \in \mathcal{S}\}$  denotes the features in subset  $\mathcal{S}$ ,  $\mathbf{x}_{\bar{\mathcal{S}}} = \{x_j : j \in \bar{\mathcal{S}}\}$  denotes the features outside  $\mathcal{S}$ , that is,  $\bar{\mathcal{S}} = \mathcal{M} \setminus \mathcal{S}$ , and  $p(\mathbf{x}_{\bar{\mathcal{S}}} | \mathbf{x}_{\mathcal{S}} = \mathbf{x}_{\mathcal{S}}^*)$  is the conditional density of  $\mathbf{x}_{\bar{\mathcal{S}}}$  given  $\mathbf{x}_{\mathcal{S}} = \mathbf{x}_{\mathcal{S}}^*$ . The conditional expectation summarises the whole probability distribution, it is the most common estimator in prediction applications, and it is also the minimiser of the commonly used squared error loss function. Strictly speaking, the notation of (2) only holds for continuous features, and the integral should be replaced by sums for discrete or categorical features in  $\mathbf{x}_{\bar{\mathcal{S}}}$ , if there are any. This contribution function is also used by, for example, Aas, Jullum, et al. (2021), Aas, Nagler, et al. (2021), H. Chen et al. (2020), Frye et al. (2021), and Redelmeier et al. (2020). In practice, the contribution function needs to be empirically approximated by, e.g., Monte Carlo integration. That is,

$$v(\mathcal{S}) \approx \hat{v}(\mathcal{S}) = \frac{1}{K} \sum_{k=1}^K f(\mathbf{x}_{\bar{\mathcal{S}}}^{(k)}, \mathbf{x}_{\mathcal{S}}^*), \quad (3)$$

where  $f$  is the machine learning model and  $\mathbf{x}_{\bar{\mathcal{S}}}^{(k)} \sim p(\mathbf{x}_{\bar{\mathcal{S}}} | \mathbf{x}_{\mathcal{S}} = \mathbf{x}_{\mathcal{S}}^*)$ , for  $k = 1, 2, \dots, K$ .

Lundberg and Lee (2017) assume feature independence, i.e.,  $p(\mathbf{x}_{\bar{\mathcal{S}}} | \mathbf{x}_{\mathcal{S}} = \mathbf{x}_{\mathcal{S}}^*) = p(\mathbf{x}_{\bar{\mathcal{S}}})$ , which means that  $\mathbf{x}_{\bar{\mathcal{S}}}^{(k)}$  can be randomly sampled from the training set. However, in observational studies, the features are rarely statistically independent. Thus, the **independence** approach may lead to incorrect explanations for real data, as discussed in, e.g., Aas, Jullum, et al. (2021), Frye et al. (2021), and Merrick and Taly (2020). Aas, Jullum, et al. (2021), Aas, Nagler, et al. (2021), and Redelmeier et al. (2020) use different methods from statistics to model the feature dependencies and generate the conditional samples  $\mathbf{x}_{\bar{\mathcal{S}}}^{(k)} \sim p(\mathbf{x}_{\bar{\mathcal{S}}} | \mathbf{x}_{\mathcal{S}} = \mathbf{x}_{\mathcal{S}}^*)$ .

The aforementioned approaches need to estimate the conditional distributions for all feature combinations, i.e.,  $p(\mathbf{x}_{\bar{\mathcal{S}}} | \mathbf{x}_{\mathcal{S}} = \mathbf{x}_{\mathcal{S}}^*)$  for all  $\mathcal{S} \subseteq \mathcal{M}$ . The number of unique feature combinations is  $2^M$ , hence, the number of conditional distributions to model increases exponentially with the number of features. Thus, the methods above have to train  $2^M$  different models,

which eventually becomes computationally intractable. The method we propose in Section 3 comes from the machine learning community and can model all the  $2^M$  different conditional distributions simultaneously with a single variational autoencoder.

### 3 Variational Autoencoder with Arbitrary Conditioning

The methodology of the *variational autoencoder with arbitrary conditioning* (VAEAC) (Ivanov et al. 2019) is an extension of the *conditional variational autoencoder* (CVAE) (Sohn et al. 2015), which is a special type of *variational autoencoder* (VAE) (Kingma and Welling 2014; Rezende et al. 2014). If the concept of VAEs is unfamiliar to the reader, we recommend reading Kingma and Welling (2019, Ch. 1 & 2). These chapters give a motivational introduction to VAEs and lay a solid technical foundation which is necessary to understand the methodology of VAEAC.

The goal of the VAE is to give a probabilistic representation of the true unknown distribution  $p(\mathbf{x})$ , while the CVAE does the same for the conditional distribution  $p(\mathbf{x}_{\bar{\mathcal{S}}}|\mathbf{x}_{\mathcal{S}} = \mathbf{x}_{\mathcal{S}}^*)$ , for a specific subset  $\mathcal{S} \subseteq \mathcal{M}$  of features. The VAEAC generalizes this methodology to all conditional distributions  $p(\mathbf{x}_{\bar{\mathcal{S}}}|\mathbf{x}_{\mathcal{S}} = \mathbf{x}_{\mathcal{S}}^*)$ , for all possible feature subsets  $\mathcal{S} \subseteq \mathcal{M}$  simultaneously.

In this paper, we present the VAEAC methodology for the Shapley value setting in the conventional Shapley value notation used in Section 2. The VAEAC consists of three fully connected feedforward neural networks (NNs) denoted the *encoder*<sup>1</sup>  $p_{\phi}$ , *masked encoder*  $p_{\psi}$ , and *decoder*  $p_{\theta}$ .<sup>2</sup> The encoder is only used during training to guide the fitting of the masked encoder. In test time, when we generate conditional samples from the estimated  $p(\mathbf{x}_{\bar{\mathcal{S}}}|\mathbf{x}_{\mathcal{S}} = \mathbf{x}_{\mathcal{S}}^*)$ , only the masked encoder and decoder are used. In Figure 1, we present a visual representation of a VAEAC model, and its associated NNs, which should make the following explanations of VAEAC easier to follow. We will go through an example based on Figure 1 once all notation and terminology is introduced.

#### 3.1 Overview of the VAEAC Model

Let  $p(\mathbf{x})$  denote the true, but unknown distribution of the data, where the input  $\mathbf{x}$  is an  $M$ -dimensional vector of continuous and/or categorical features. The true conditional distribution  $p(\mathbf{x}_{\bar{\mathcal{S}}}|\mathbf{x}_{\mathcal{S}})$  is usually unknown, unless strong assumptions about the data distribution  $p(\mathbf{x})$  are made. Here  $\mathbf{x}_{\mathcal{S}}$  and  $\mathbf{x}_{\bar{\mathcal{S}}}$  are denoted the *observed features* (that we condition on) and *unobserved features* of  $\mathbf{x}$ , respectively. Ivanov et al. (2019) say that the unobserved features  $\mathbf{x}_{\bar{\mathcal{S}}}$  are *masked* by the *mask*  $\bar{\mathcal{S}}$ .

The VAEAC model estimates a probabilistic representation  $p_{\psi, \theta}(\mathbf{x}_{\bar{\mathcal{S}}}|\mathbf{x}_{\mathcal{S}}, \bar{\mathcal{S}})$  of the true unknown conditional distribution  $p(\mathbf{x}_{\bar{\mathcal{S}}}|\mathbf{x}_{\mathcal{S}})$ , for a given  $\mathbf{x}_{\mathcal{S}} = \mathbf{x}_{\mathcal{S}}^*$  and an arbitrary  $\mathcal{S} \subseteq \mathcal{M}$ . Here,  $\psi$  and  $\theta$  denote the learned model parameters of the masked encoder and decoder, respectively. The masked encoder is an extension of the VAE methodology, which solely consists of a decoder and encoder, where the latter is parameterized by  $\phi$ . As VAEAC estimates all conditional distributions simultaneously, the trained conditional model  $p_{\psi, \theta}(\mathbf{x}_{\bar{\mathcal{S}}}|\mathbf{x}_{\mathcal{S}}, \bar{\mathcal{S}})$  may be more precise for some  $\bar{\mathcal{S}}$  and less precise for others. The precision can be controlled by introducing a *masking scheme*, which is a distribution  $p(\bar{\mathcal{S}})$  over different masks/feature subsets  $\bar{\mathcal{S}}$ . The mask distribution  $p(\bar{\mathcal{S}})$  can be arbitrary or defined based on the problem at the hand. However, it should have full support over the set of all subsets of  $\mathcal{M}$ , to ensure that  $p_{\psi, \theta}(\mathbf{x}_{\bar{\mathcal{S}}}|\mathbf{x}_{\mathcal{S}}, \bar{\mathcal{S}})$  can evaluate arbitrary conditions. We discuss different masking schemes for the Shapley value setting in Appendix C.3.

<sup>1</sup>In *variational inference* notation, the variational distributions are often denoted by  $q$  instead of  $p$ .

<sup>2</sup>Ivanov et al. (2019) call them the *proposal network*, *prior network*, and *generative network*, respectively.

The log-likelihood objective function of the VAEAC model is therefore

$$\mathbb{E}_{p(\mathbf{x})}\mathbb{E}_{p(\bar{\mathcal{S}})}[\log p_{\psi,\theta}(\mathbf{x}_{\bar{\mathcal{S}}}|\mathbf{x}_{\mathcal{S}},\bar{\mathcal{S}})]. \quad (4)$$

Note that if  $\bar{\mathcal{S}} = \mathcal{M}$  (all features are unobserved) then (4) becomes the objective function of the VAE (Kingma and Welling 2014; Rezende et al. 2014), and if  $p(\bar{\mathcal{S}}) = 1$  for some fixed  $\bar{\mathcal{S}}$  (i.e., one specific mask) then (4) corresponds to the objective function of CVAE (Sohn et al. 2015). Thus, VAEAC generalizes both the VAE and CVAE.

### 3.2 Model Description

The generative process of VAEAC is a two-step procedure, similar to that of VAE and CVAE. First, we generate a latent representation  $\mathbf{z} \sim p_{\psi}(\mathbf{z}|\mathbf{x}_{\mathcal{S}},\bar{\mathcal{S}}) \in \mathbb{R}^d$  using the masked encoder, where the dimension of the latent space,  $d$ , is specified by the user of VAEAC. Second, we sample the unobserved features from  $\mathbf{x}_{\bar{\mathcal{S}}} \sim p_{\theta}(\mathbf{x}_{\bar{\mathcal{S}}}|\mathbf{z},\mathbf{x}_{\mathcal{S}},\bar{\mathcal{S}})$  using the decoder. This process marginalizes over the latent variables, resulting in the following distribution over the unobserved features:

$$p_{\psi,\theta}(\mathbf{x}_{\bar{\mathcal{S}}}|\mathbf{x}_{\mathcal{S}},\bar{\mathcal{S}}) = \mathbb{E}_{\mathbf{z} \sim p_{\psi}(\mathbf{z}|\mathbf{x}_{\mathcal{S}},\bar{\mathcal{S}})}[p_{\theta}(\mathbf{x}_{\bar{\mathcal{S}}}|\mathbf{z},\mathbf{x}_{\mathcal{S}},\bar{\mathcal{S}})], \quad (5)$$

similar to the procedures in VAEs and CVAEs.

The continuous latent variables of the masked encoder are assumed to be multivariate Gaussian with a diagonal covariance matrix, i.e.,  $p_{\psi}(\mathbf{z}|\mathbf{x}_{\mathcal{S}},\bar{\mathcal{S}}) = \mathcal{N}_d(\mathbf{z}|\boldsymbol{\mu}_{\psi}(\mathbf{x}_{\mathcal{S}},\bar{\mathcal{S}}), \text{diag}[\boldsymbol{\sigma}_{\psi}^2(\mathbf{x}_{\mathcal{S}},\bar{\mathcal{S}})])$ . Here  $\boldsymbol{\mu}_{\psi}$  and  $\boldsymbol{\sigma}_{\psi}$  are the  $d$ -dimensional outputs of the NN for the masked encoder  $p_{\psi}$ . As the output nodes of NNs are unbounded, we apply the soft-plus function<sup>3</sup> to  $\boldsymbol{\sigma}_{\psi}$  to ensure that the standard deviations are positive. We directly send any continuous features of  $\mathbf{x}_{\mathcal{S}}$  to the masked encoder, while any categorical features are one-hot encoded first. One-hot encoding is the most widely used coding scheme for categorical features in NNs (Potdar et al. 2017). Note that the components of the latent representation  $\mathbf{z}$  are conditionally independent given  $\mathbf{x}_{\mathcal{S}}$  and  $\bar{\mathcal{S}}$ .

The encoder is also assumed to be a multivariate Gaussian distribution with a diagonal covariance matrix, that is,  $p_{\phi}(\mathbf{z}|\mathbf{x},\bar{\mathcal{S}}) = \mathcal{N}_d(\mathbf{z}|\boldsymbol{\mu}_{\phi}(\mathbf{x},\bar{\mathcal{S}}), \text{diag}[\boldsymbol{\sigma}_{\phi}^2(\mathbf{x},\bar{\mathcal{S}})])$ . The encoder is conditioned on the full observation  $\mathbf{x}$ , in contrast to the masked encoder which is solely conditioned on the observed features  $\mathbf{x}_{\mathcal{S}}$ . Furthermore, it also uses one-hot encoding to handle any categorical features. The encoder is only used during the training process of VAEAC, which will become clear in Section 3.3.

The decoder  $p_{\theta}(\mathbf{x}_{\bar{\mathcal{S}}}|\mathbf{z},\mathbf{x}_{\mathcal{S}},\bar{\mathcal{S}})$  is also assumed to follow a multivariate Gaussian structure for the continuous features of  $\mathbf{x}_{\bar{\mathcal{S}}}$ , i.e.,  $p_{\theta}(\mathbf{x}_{\bar{\mathcal{S}}}|\mathbf{z},\mathbf{x}_{\mathcal{S}},\bar{\mathcal{S}}) = \mathcal{N}(\mathbf{x}_{\bar{\mathcal{S}}}|\boldsymbol{\mu}_{\theta}(\mathbf{z},\mathbf{x}_{\mathcal{S}},\bar{\mathcal{S}}), \text{diag}[\boldsymbol{\sigma}_{\theta}^2(\mathbf{z},\mathbf{x}_{\mathcal{S}},\bar{\mathcal{S}})])$ . We discuss this assumption in Section 6. As the latent variables  $\mathbf{z}$  are continuous and  $p_{\theta}(\mathbf{x}_{\bar{\mathcal{S}}}|\mathbf{z},\mathbf{x}_{\mathcal{S}},\bar{\mathcal{S}})$  is in this case Gaussian, the distribution  $p_{\psi,\theta}(\mathbf{x}_{\bar{\mathcal{S}}}|\mathbf{x}_{\mathcal{S}},\bar{\mathcal{S}})$  in (5) can be seen as an infinite mixture of Gaussian distributions (Kingma and Welling 2019, p. 12), which is a universal approximator of densities, in the sense that any smooth density can be arbitrarily well approximated (Goodfellow, Bengio, et al. 2016, p. 65).

The Gaussian structure is incompatible with categorical features, e.g., feature  $x_j$  with  $L$  categories. When working with multi-class features and NNs, it is common practice to let the outputs  $\mathbf{w}_{j,\theta}(\mathbf{z},\mathbf{x}_{\mathcal{S}},\bar{\mathcal{S}})$  of the NN be the logits of the probabilities for each category. That is,  $\mathbf{w}_{j,\theta}(\mathbf{z},\mathbf{x}_{\mathcal{S}},\bar{\mathcal{S}}) = \text{logit}(\mathbf{p}_j) = \log[\mathbf{p}_j/(1 - \mathbf{p}_j)]$  is an  $L$ -dimensional vector of the logits for each of the  $L$  categories for the categorical  $j$ th feature. As logits are unbounded, we use the softmax function<sup>4</sup> to map the logits to probabilities in  $(0,1)$ . Finally, we use the categorical distribution with  $L$  categories to model each of the categorical features, i.e.,

<sup>3</sup>softplus( $x$ ) =  $\log(1 + \exp(x))$ .

<sup>4</sup>softmax( $\mathbf{w}_{j,\theta}$ ) <sub>$i$</sub>  =  $\exp\{\mathbf{w}_{j,\theta,i}\} / \sum_{l=1}^L \exp\{\mathbf{w}_{j,\theta,l}\}$ , for  $i = 1, \dots, L$ .

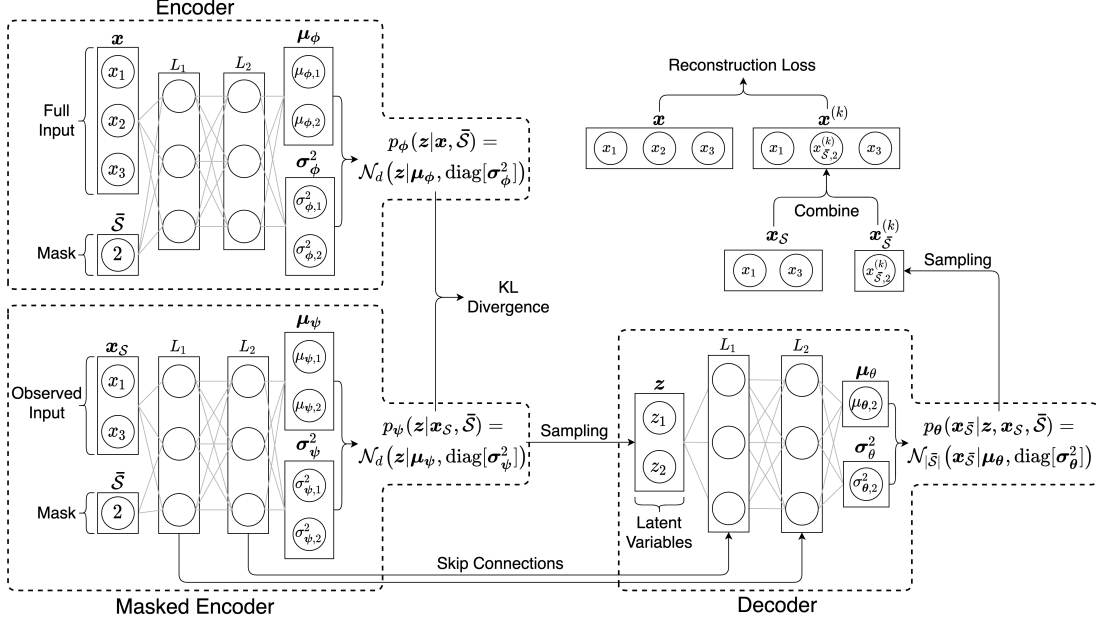


**Figure 1:** A visual representation of the VAEAC model used in the example given at the end of Section 3.2. The model has parameters `depth` = 2, `width` = 3,  $d = \text{latent\_dim} = 2$  for an  $M = 3$ -dimensional continuous input  $\mathbf{x} = \{x_1, x_2, x_3\}$ , with coalition  $\mathcal{S} = \{1, 3\}$  and mask  $\bar{\mathcal{S}} = \{2\}$ . The *Encoder*, *KL Divergence*, and *Reconstruction Loss* are related to the training of VAEAC, and not used during test time. Only the *Masked Encoder* and *Decoder* are used in test time to generate the samples  $x_{\bar{\mathcal{S}}}^{(k)} \sim p_{\psi, \theta}(\mathbf{x}_{\bar{\mathcal{S}}} | \mathbf{x}_{\mathcal{S}} = \mathbf{x}_{\mathcal{S}}^*)$ , for  $k = 1, \dots, K$ , where  $K$  is the number of Monte Carlo samples.

$x_j \sim \text{Cat}[\text{Softmax}(\mathbf{w}_{j, \theta}(\mathbf{z}, \mathbf{x}_{\mathcal{S}}, \bar{\mathcal{S}}))]$ . Note that even though we used one-hot encoding in the encoders, the sampled categorical features will be on the original categorical form and *not* in the one-hot encoded representation. Furthermore, note that the components of  $\mathbf{x}_{\bar{\mathcal{S}}}$  are conditionally independent given  $\mathbf{z}, \mathbf{x}_{\mathcal{S}}$ , and  $\bar{\mathcal{S}}$ .

We now give a walk-through of the VAEAC model shown in Figure 1. The notation and representation of the network architecture is simplified for ease of understanding, but the complete implementation details are found in Appendix C.1. The aim is to sample  $x_{\bar{\mathcal{S}}}^{(k)} \sim p_{\psi, \theta}(\mathbf{x}_{\bar{\mathcal{S}}} | \mathbf{x}_{\mathcal{S}} = \mathbf{x}_{\mathcal{S}}^*)$ , for  $k = 1, \dots, K$ , where  $K$  is the number of Monte Carlo samples in (3). Let the  $M = 3$ -dimensional continuous input be  $\mathbf{x} = \{x_1, x_2, x_3\}$ , while the coalition and mask are  $\mathcal{S} = \{1, 3\}$  and  $\bar{\mathcal{S}} = \{2\}$ , respectively. Thus, the associated observed and unobserved feature vectors are  $\mathbf{x}_{\mathcal{S}} = \{x_1, x_3\}$  and  $\mathbf{x}_{\bar{\mathcal{S}}} = \{x_2\}$ , respectively. The conditional samples  $x_{\bar{\mathcal{S}}}^{(k)}$  are generated by first sending  $\mathbf{x}_{\mathcal{S}}$  and  $\bar{\mathcal{S}}$  through the masked encoder. This yields the latent probabilistic representation  $p_{\psi}(\mathbf{z} | \mathbf{x}_{\mathcal{S}}, \bar{\mathcal{S}}) = \mathcal{N}_d(\mathbf{z} | \boldsymbol{\mu}_{\psi}(\mathbf{x}_{\mathcal{S}}, \bar{\mathcal{S}}), \text{diag}[\boldsymbol{\sigma}_{\psi}^2(\mathbf{x}_{\mathcal{S}}, \bar{\mathcal{S}})])$ , where we have set  $d = 2$ . We sample  $K$  latent representations  $\mathbf{z}^{(k)} \sim p_{\psi}(\mathbf{z} | \mathbf{x}_{\mathcal{S}}, \bar{\mathcal{S}})$ , which are then sent through the decoder. This yields  $K$  versions of  $p_{\theta}(\mathbf{x}_{\bar{\mathcal{S}}} | \mathbf{z}^{(k)}, \mathbf{x}_{\mathcal{S}}, \bar{\mathcal{S}}) = \mathcal{N}(\mathbf{x}_{\bar{\mathcal{S}}} | \boldsymbol{\mu}_{\theta}(\mathbf{z}^{(k)}, \mathbf{x}_{\mathcal{S}}, \bar{\mathcal{S}}), \text{diag}[\boldsymbol{\sigma}_{\theta}^2(\mathbf{z}^{(k)}, \mathbf{x}_{\mathcal{S}}, \bar{\mathcal{S}})])$ , for which we sample *one* observation from each, that is,  $x_{\bar{\mathcal{S}}}^{(k)} \sim p_{\theta}(\mathbf{x}_{\bar{\mathcal{S}}} | \mathbf{z}^{(k)}, \mathbf{x}_{\mathcal{S}}, \bar{\mathcal{S}})$ . Ivanov et al. (2019) call this process of repeatedly generating the missing values  $\mathbf{x}_{\bar{\mathcal{S}}}$  based on  $\mathbf{x}_{\mathcal{S}}$  for *missing features multiple imputation*.

### 3.3 Training the VAEAC Model

The model parameters  $\psi$  and  $\theta$  are not easily tuned by maximizing the log-likelihood (4), as this optimization problem is challenging due to intractable posterior inference. Kingma and Welling (2019, Ch. 2) discuss the same issue for the VAE. The optimization problem is bypassed by *variational inference*<sup>5</sup> (Blei et al. 2017) where we rather optimize the *variational lower bound* (VLB). The VLB is also called the *evidence lower bound* (ELBO) in variational inference. The main contribution of Kingma and Welling (2014) is their reparameterization trick of VAE’s latent variables. This allows for efficient fitting of VAE’s model parameters and optimization of the VLB by using backpropagation and stochastic gradient descent (Goodfellow, Bengio, et al. 2016, Ch. 6 & 8). The same type of techniques are used to optimize VAEAC’s model parameters.

Like for VAEs, we can derive a variational lower bound for VAEAC:

$$\begin{aligned} \log p_{\psi, \theta}(\mathbf{x}_{\bar{S}} | \mathbf{x}_S, \bar{S}) &= \mathbb{E}_{p_{\phi}(\mathbf{z} | \mathbf{x}, \bar{S})} \left[ \log \frac{p_{\psi, \theta}(\mathbf{x}_{\bar{S}}, \mathbf{z} | \mathbf{x}_S, \bar{S})}{p_{\phi}(\mathbf{z} | \mathbf{x}, \bar{S})} \right] + \mathbb{E}_{p_{\phi}(\mathbf{z} | \mathbf{x}, \bar{S})} \left[ \log \frac{p_{\phi}(\mathbf{z} | \mathbf{x}, \bar{S})}{p_{\psi, \theta}(\mathbf{z} | \mathbf{x}, \bar{S})} \right] \\ &\geq \mathbb{E}_{p_{\phi}(\mathbf{z} | \mathbf{x}, \bar{S})} [\log p_{\theta}(\mathbf{x}_{\bar{S}} | \mathbf{z}, \mathbf{x}_S, \bar{S})] - D_{\text{KL}}(p_{\phi}(\mathbf{z} | \mathbf{x}, \bar{S}) \parallel p_{\psi}(\mathbf{z} | \mathbf{x}_S, \bar{S})) \\ &= \mathcal{L}_{\text{VAEAC}}(\mathbf{x}, \bar{S} | \theta, \psi, \phi), \end{aligned} \quad (6)$$

where the Kullback–Leibler divergence  $D_{\text{KL}}$ , for two continuous probability distributions  $p$  and  $q$ , is given by  $D_{\text{KL}}(p \parallel q) = \int_{-\infty}^{\infty} p(\mathbf{z}) \log \frac{p(\mathbf{z})}{q(\mathbf{z})} d\mathbf{z} = \mathbb{E}_{p(\mathbf{z})} \left[ \log \frac{p(\mathbf{z})}{q(\mathbf{z})} \right] \geq 0$ . We obtain a *tight* variational lower bound if  $p_{\phi}(\mathbf{z} | \mathbf{x}, \bar{S})$  is close to  $p_{\psi, \theta}(\mathbf{z} | \mathbf{x}, \bar{S})$  with respect to the Kullback–Leibler divergence. The full derivation of (6) is presented in Appendix B.

Instead of maximizing the log-likelihood in (4), we rather have the following variational lower bound optimization problem for VAEAC:

$$\max_{\theta, \psi, \phi} \mathbb{E}_{p(\mathbf{x})} \mathbb{E}_{p(\bar{S})} [\mathcal{L}_{\text{VAEAC}}(\mathbf{x}, \bar{S} | \theta, \psi, \phi)] = \min_{\theta, \psi, \phi} \mathbb{E}_{p(\mathbf{x})} \mathbb{E}_{p(\bar{S})} [-\mathcal{L}_{\text{VAEAC}}(\mathbf{x}, \bar{S} | \theta, \psi, \phi)], \quad (7)$$

which is optimized similarly as VAEs. Since we assumed  $p_{\phi}$  and  $p_{\psi}$  to be multivariate Gaussians, we have a closed-form expression for the Kullback–Leibler divergence in (6). The parameters  $\psi$  and  $\theta$  can be directly optimized using Monte Carlo estimates, backpropagation, and stochastic gradient descent.

The gradient of  $\mathcal{L}_{\text{VAEAC}}(\mathbf{x}, \bar{S} | \theta, \psi, \phi)$  with respect to the variational parameter  $\phi$  is more complicated to compute as the expectation in (6) is taken with respect to  $p_{\phi}(\mathbf{z} | \mathbf{x}, \bar{S})$ , which is a function of  $\phi$ . However, the gradient can be efficiently estimated using the reparameterization trick of Kingma and Welling (2014). The trick is to rewrite the latent variable vector as  $\mathbf{z} = \boldsymbol{\mu}_{\phi}(\mathbf{x}, \bar{S}) + \boldsymbol{\epsilon} \boldsymbol{\sigma}_{\phi}(\mathbf{x}, \bar{S})$ , where  $\boldsymbol{\epsilon} \sim \mathcal{N}_d(0, I)$  and  $\boldsymbol{\mu}$  and  $\boldsymbol{\sigma}$  are deterministic functions parameterized by the NN of the encoder. That is, the randomness in  $\mathbf{z}$  has been *externalized* to  $\boldsymbol{\epsilon}$  by reparameterizing  $\mathbf{z}$  as a deterministic and differentiable function of  $\phi$ ,  $\mathbf{x}$ ,  $\bar{S}$ , and the random variable  $\boldsymbol{\epsilon}$ . Thus, the gradient is

$$\begin{aligned} \frac{\partial \mathcal{L}_{\text{VAEAC}}(\mathbf{x}, \bar{S} | \theta, \psi, \phi)}{\partial \phi} &= \mathbb{E}_{\boldsymbol{\epsilon} \sim \mathcal{N}_d(0, I)} \left[ \frac{\partial}{\partial \phi} \log p_{\theta}(\mathbf{x}_{\bar{S}} | \boldsymbol{\mu}_{\phi}(\mathbf{x}, \bar{S}) + \boldsymbol{\epsilon} \boldsymbol{\sigma}_{\phi}(\mathbf{x}, \bar{S}), \mathbf{x}_S, \bar{S}) \right] \\ &\quad - \frac{\partial}{\partial \phi} D_{\text{KL}}(p_{\phi}(\mathbf{z} | \mathbf{x}, \bar{S}) \parallel p_{\psi}(\mathbf{z} | \mathbf{x}_S, \bar{S})), \end{aligned}$$

where the first term is estimated using Monte Carlo sampling, while we use the closed-form expression mentioned above for the second term.

<sup>5</sup>Also called *variational Bayes* and VAEs belong to the family of *variational Bayesian methods*.



Furthermore, **VAEAC** uses *skip connections* with concatenation between the layers of the masked encoder and the decoder, as seen in Figure 1. Skip connections are architectural tools used to ensure effective learning of model parameters in deep NNs (Mao et al. 2016; Ronneberger et al. 2015). They allow for efficient computation of gradients during backpropagation for all layers in the masked encoder. Without skip connections, the gradients used to update the masked encoder would have to go through the latent space.

### 3.3.1 Prior in Latent Space

When optimizing the variational lower bound in (7), there are no restrictions on the estimated mean  $\boldsymbol{\mu}_\psi$  and on the size of the standard deviation  $\boldsymbol{\sigma}_\psi$  in the masked encoder. That is, they can grow to infinity and cause numerical instabilities. We follow Ivanov et al. (2019) and solve this problem by adding a normal prior on  $\boldsymbol{\mu}_\psi$  and gamma prior on  $\boldsymbol{\sigma}_\psi$  to prevent divergence. That is, we redefine  $p_\psi(\mathbf{z}, \boldsymbol{\mu}_\psi, \boldsymbol{\sigma}_\psi | \mathbf{x}_S, \bar{\mathcal{S}})$  as

$$p_\psi(\mathbf{z}, \boldsymbol{\mu}_\psi, \boldsymbol{\sigma}_\psi | \mathbf{x}_S, \bar{\mathcal{S}}) = \mathcal{N}_d(\mathbf{z} | \boldsymbol{\mu}_\psi(\mathbf{x}_S, \bar{\mathcal{S}}), \text{diag}[\boldsymbol{\sigma}_\psi^2(\mathbf{x}_S, \bar{\mathcal{S}})]) \mathcal{N}(\boldsymbol{\mu}_\psi | 0, \sigma_\mu^2) \Gamma(\boldsymbol{\sigma}_\psi | 1 + \sigma_\sigma^{-1}, \sigma_\sigma^{-1}), \quad (8)$$

where  $\Gamma$  is the gamma distribution with shape parameter  $1 + \sigma_\sigma^{-1}$  and rate parameter  $\sigma_\sigma^{-1}$ , thus, the mean is  $1 + \sigma_\sigma$  and the variance is  $\sigma_\sigma(1 + \sigma_\sigma)$ . The hyperparameters  $\sigma_\mu$  and  $\sigma_\sigma$  are set to be large, not to affect the learning process significantly.

When re-deriving the variational lower bound (6) with the updated version of  $p_\psi$  with priors (8), we get two additional regularizing terms in the VLB, after removing fixed constants. Thus, we maximize the following VLB in (7):

$$\begin{aligned} \mathcal{L}_{\text{VAEAC}}(\mathbf{x}, \bar{\mathcal{S}} | \boldsymbol{\theta}, \boldsymbol{\psi}, \boldsymbol{\phi}) = & \mathbb{E}_{p_\phi(\mathbf{z} | \mathbf{x}, \bar{\mathcal{S}})} [\log p_\theta(\mathbf{x}_{\bar{\mathcal{S}}} | \mathbf{z}, \mathbf{x}_S, \bar{\mathcal{S}})] - D_{\text{KL}}(p_\phi(\mathbf{z} | \mathbf{x}, \bar{\mathcal{S}}) \parallel p_\psi(\mathbf{z} | \mathbf{x}_S, \bar{\mathcal{S}})) \\ & - \frac{\boldsymbol{\mu}_\psi^2}{2\sigma_\mu^2} + \frac{1}{\sigma_\sigma} (\log(\boldsymbol{\sigma}_\psi) - \boldsymbol{\sigma}_\psi). \end{aligned}$$

Large values of  $\boldsymbol{\mu}_\psi^2$  and  $\boldsymbol{\sigma}_\psi$  decrease the new VLB through its last two terms, but their magnitude is controlled by the hyperparameters  $\sigma_\mu$  and  $\sigma_\sigma$ . Ivanov et al. (2019) obtain identical regularizers, but there is a misprint in the shape parameter of their specified gamma prior.

## 4 Simulation Studies

A major problem of evaluating explanation methods is that there is in general no ground truth for authentic real-world data. To verify and compare explanation methods, we have to use simulated data for which we can compute the true Shapley values. In this section, we conduct and discuss two types of simulation studies: continuous data (Section 4.2) and mixed data (Section 4.3). Simulation studies limited to categorical features have also been investigated, but as real-world data sets are seldom restricted to only categorical features, we rather report the corresponding results in Appendix D. See Appendix C for the choice of **VAEAC**'s hyperparameters and an investigation on the effect of different masking schemes  $p(\bar{\mathcal{S}})$ .

For the continuous setting, we compare the **VAEAC** approach with the **independence** method from Lundberg and Lee (2017), the **empirical**, **Gaussian**, and **copula** approaches from Aas, Jullum, et al. (2021), and the **ctree** method from Redelmeier et al. (2020). The methods are briefly described in Appendix A. For the mixed data setting, with continuous and categorical features, the methods of Aas, Jullum, et al. (2021) are dismissed as they lack native support for categorical data. Use of feature encodings, such as one-hot encoding, is possible, but drastically increase the computational time, due to the detour of estimating Shapley values for each dummy

feature. This *external* use of one-hot encoding must not be confused with VAEAC’s *internal* use of one-hot encoding described in Section 3.2.

All mentioned methodologies are implemented in the software package **shapr** (Sellereite and Jullum 2019) in the R programming language (R Core Team 2020), and we use the default hyperparameters. Ivanov et al. (2019) have implemented VAEAC in Python (Python Core Team 2020), see <https://github.com/tigvarts/vaeac>. We have made changes to their implementation and used **reticulate** (Ushey et al. 2020) to run Python code in R, such that the VAEAC approach runs on top of the **shapr**-package. Our version of VAEAC can be accessed on <https://github.com/LHBO/ShapleyValuesVAEAC>.

## 4.1 Evaluation Method

We use the mean absolute error (MAE) as the performance measure to evaluate the precision of the estimated Shapely values using method  $q$ . The MAE is taken across both the feature and test sample space, and it is defined as

$$\text{MAE}(\text{method } q) = \frac{1}{N_{\text{test}}} \sum_{i=1}^{N_{\text{test}}} \frac{1}{M} \sum_{j=1}^M |\phi_{j,\text{true}}(\mathbf{x}^{(i)}) - \phi_{j,q}(\mathbf{x}^{(i)})|. \quad (9)$$

Here  $\mathbf{x}^{(i)}$  is the  $i$ th  $M$ -dimensional test observation, for  $i = 1, \dots, N_{\text{test}}$ , while  $\phi_{j,\text{true}}(\mathbf{x}^{(i)})$  denotes the true  $j$ th Shapley value for the prediction  $f(\mathbf{x}^{(i)})$  and  $\phi_{j,q}(\mathbf{x}^{(i)})$  is the corresponding estimate using method  $q$ .

In real-world settings, we cannot compute the true Shapley values  $\phi_{j,\text{true}}(\mathbf{x}^{(i)})$  as the underlying data generating process is unknown. However, in the following simulation studies, we can compute  $\phi_{j,\text{true}}(\mathbf{x}^{(i)})$  with arbitrary precision as the true conditional distributions of the data are known.

## 4.2 Simulation Study: Continuous Data

For the first simulation study, we consider  $M = 10$ -dimensional continuous, positive, multi-variate Burr distributed data. See Appendix E.1 for an introduction to the Burr distribution. As the Burr distribution has known conditional distributions, we can compute the true Shapley values with arbitrary precision by using Monte Carlo integration. The simulation study is similar to Aas, Nagler, et al. (2021), but we rather let the predictive model be an XGBoost model (T. Chen et al. 2015). In addition, we use slightly different parameters in the Burr distribution for more realistic data.

We perform 3 experiments with different training sample sizes  $N_{\text{train}} \in \{100, 1000, 5000\}$ , while  $N_{\text{test}} = 100$ . The smallest training size is chosen to demonstrate that VAEAC works well even for limited data, in contrast to the common belief that neural networks need large amounts of data to be properly fitted. For each training size, we let the scale parameter  $\kappa$  of the Burr distribution be  $\kappa \in \{1, 2, 3\}$ , while the remaining parameters are taken from Aas, Nagler, et al. (2021), i.e.,  $\mathbf{b} = (2, 4, 6, 2, 4, 6, 2, 4, 6, 6)$  and  $\mathbf{r} = (1, 3, 5, 1, 3, 5, 1, 3, 5, 5)$ . The three values of  $\kappa$  correspond to a pair-wise Kendall’s  $\tau$  of 0.25, 0.20 and 0.14, respectively.

The response is generated according to the same non-linear and heteroscedastic function as in Aas, Nagler, et al. (2021). That is,

$$y = u_1 u_2 \exp(1.8 u_3 u_4) + u_5 u_6 \exp(1.8 u_7 u_8) + u_9 \exp(1.8 u_{10}) + 0.5(u_1 + u_5 + u_9)\epsilon, \quad (10)$$

where  $\epsilon \stackrel{\text{iid}}{\sim} \mathcal{N}(0, 1)$  and  $u_j = F_j(x_j)$ , for  $j = 1, 2, \dots, M$ . Here  $\mathbf{x}$  is multivariate Burr distributed and  $F_j$  is the true parametric (cumulative) distribution function for the  $j$ th feature. Thus, each

$M$	Rep	$N_{\text{train}}$	Method	$\overline{\text{MAE}}$ for each $\kappa$			
				1	2	3	CPU
10	20	100	Independence	0.2694	0.1916	0.1630	0.40
			Empirical	0.1633	0.1585	0.1661	0.39
			Gaussian	0.1349	0.1007	<b>0.0949</b>	11.11
			Copula	0.1292	0.1026	0.0968	17.26
			Ctree	0.1866	0.1650	0.1497	10.07
			VAEAC	<b>0.1102</b>	<b>0.0934</b>	0.0968	7.90
10	20	1000	Independence	0.2730	0.2224	0.1840	3.19
			Empirical	0.0890	0.0741	0.0751	3.15
			Gaussian	0.1196	0.0793	0.0664	11.08
			Copula	0.1087	0.0929	0.0767	17.80
			Ctree	0.0897	0.0871	0.0815	11.17
			VAEAC	<b>0.0666</b>	<b>0.0594</b>	<b>0.0527</b>	9.59
10	20	5000	Independence	0.2760	0.2298	0.1948	4.58
			Empirical	0.0742	0.0479	0.0450	4.49
			Gaussian	0.1375	0.0794	0.0655	11.08
			Copula	0.1069	0.0916	0.0775	20.24
			Ctree	0.0548	0.0552	0.0546	19.18
			VAEAC	<b>0.0418</b>	<b>0.0396</b>	<b>0.0413</b>	18.36

**Table 1:** Table of average MAE over 20 repetition for the  $M = 10$ -dimensional continuous Burr( $\kappa$ ) simulations with  $K = 250$  Monte Carlo samples. Lower  $\kappa$  means higher feature dependence. VAEAC is clearly the best method as it yields significantly lower MAE than the other methods. The last column reports the average CPU time in minutes needed to generate the estimated Shapley values for  $N_{\text{test}} = 100$  test observations, that is, one repetition for one value of  $\kappa$ .

$u_j$  is uniformly distributed between 0 and 1, but the dependence structure between the features is kept.

We repeat each of the 9 experiments 20 times for each approach and report the average MAE over those repetitions. Hence, the quality of the estimated Shapley values is evaluated based on a total of 2000 test observations. For each approach, we use  $K = 250$  Monte Carlo samples in (3). We experimented with larger values of  $K$  and saw a marginal decrease in MAE, but at the cost of increased computation time, as reported in Appendix F. Thus, we found  $K = 250$  to be a suitable trade-off between precision and computation time. Furthermore, we sample new data for each repetition to reduce the influence of the exact shape of the fitted predictive model. An outline of the procedure is given in Appendix E.1.

The results of the experiments are shown in Table 1. The best performing approach is indicated with bold font for each experiment. We see that VAEAC is the most accurate method in 8 out of 9 experiments, and it often outperforms the other methods by a significant margin.

For the larger sample sizes  $N_{\text{train}} \in \{1000, 5000\}$ , we see that VAEAC is uncontested. For the very small training size  $N_{\text{train}} = 100$ , VAEAC is clearly best for  $\kappa \in \{1, 2\}$ , but the results of Gaussian, copula, and VAEAC are indistinguishable for  $\kappa = 3$ . The VAEAC model used in these simulations consists of 18724 parameters, see Appendix C.2, which might sound enormous considering the small training set. However, recall from Section 3 that each observation can be masked in  $2^M$  different ways, hence, VAEAC’s parameters are fitted based on  $2^M \times N_{\text{train}}$  possible different observations.

The evaluation of the methods should not be limited to their accuracy, but also include their computational complexity. The last column of Table 1 displays the average CPU time (in minutes) needed for each approach to explain  $N_{\text{test}} = 100$  test observations. The CPU times will vary depending on software and hardware. We have run the simulations on a computer running Red Hat Enterprise Linux 8.4 with an Intel(R) Core(TM) i3-8100 CPU @ 3.60GHz and 16GB DDR4 RAM. The **independence** and **empirical** approaches are the fastest methods, but they yield particularly bad results for small training sets. The **VAEAC** approach is faster than **copula** and **ctree** for all training sizes, and faster than **Gaussian** for  $N_{\text{train}} \in \{100, 1000\}$ . When  $N_{\text{train}}$  increases, most methods yield larger computational times. The reason for **VAEAC**'s time increase is related to its training phase and not the sampling. When we train the NNs in **VAEAC**, we have used a conservative number of epochs, see Appendix C.2. Thus, when  $N_{\text{train}}$  increases, each epoch takes longer time to run. Optimal choice of hyperparameters (epochs, learning rate, NN architecture) and use of early stopping regimes might decrease the training time without loss of accuracy. The **VAEAC** approach uses approximately 7.4 minutes to generate the conditional samples, while the remainder of the CPU times given in Table 1 are used for training the model.

### 4.3 Simulation Study: Mixed Data

The second type of simulation study concerns mixed data following the setup of Redelmeier et al. (2020), to which we refer for technical details on the data generating process. The essentials are presented in Appendix E.2. We only consider two experiments, in dimensions 4 and 6, respectively, outlined in Table 2, as the computational complexity of calculating the true Shapley values is intractable for larger dimensions due to numerical integration.

To generate  $M$ -dimensional dependent mixed data, we first generate  $N_{\text{train}} = 1000$  samples from  $\mathcal{N}_M(\mathbf{0}, \Sigma_\rho)$ , where the covariance matrix  $\Sigma_\rho$  is 1 on the diagonal and  $\rho$  off-diagonal. A large  $\rho$  implies high feature dependence. The categorical features are created by categorizing the first  $M_{\text{cat}}$  of the  $M$  continuous Gaussian features into  $L$  categories at certain cut-off-values, while the remaining  $M_{\text{cont}}$  continuous features are left untouched, see Table 2. The response is generated according to

$$y = \alpha + \sum_{j=1}^{M_{\text{cat}}} \sum_{l=1}^L \beta_{jl} \mathbb{I}(x_j = l) + \sum_{j=M_{\text{cat}}+1}^{M_{\text{cat}}+M_{\text{cont}}} \gamma_j x_j + \epsilon, \quad (11)$$

where the coefficients are defined in Table 2,  $\epsilon \stackrel{iid}{\sim} \mathcal{N}(0, 1)$ , and  $\mathbb{I}$  is the indicator function. We fit a linear regression model of the same form as (11), but without the error term, to act as the predictive model  $f$ .

The precision of the Shapley value estimates for the three methods are evaluated based on the MAE in (9). We use  $N_{\text{test}} = 500$  randomly sampled test observations from the joint distribution to compute the MAE, and the results are presented in Table 3. We obtain similar

$M$	$M_{\text{cont}}$	$M_{\text{cat}}$	$L$	Categorical cut-off values	$N_{\text{test}}$	$\beta_1$	$\beta_2$	$\gamma$
4	2	2	4	$(-\infty, -0.5, 0, 1, \infty)$	500	1, 0, -1, 0.5	2, 3, -1, -0.5	1, -1
6	4	2	3	$(-\infty, 0, 1, \infty)$	500	1, 0, -1	2, 3, -0.5	1, -1, 2, -0.25

**Table 2:** Table of the number of continuous and categorical features, along with the number of categories  $L$ , the associated cut-off values, and the number of test observations  $N_{\text{test}}$  for the two experiments. The last three columns display the true model parameters of (11), while  $\alpha = 1$ .

$M$	$M_{\text{cont}}$	$M_{\text{cat}}$	$L$	Rep	Method	$\overline{\text{MAE}}$ for each $\rho$						$\overline{\text{CPU}}$
						0.0	0.1	0.3	0.5	0.8	0.9	
4	2	2	4	25	Indep.	<b>0.0289</b>	0.0811	0.2203	0.3541	0.5615	0.6478	0.36
					Ctree	0.0320	<b>0.0706</b>	0.1050	0.1150	0.1052	0.0954	0.70
					VAEAC	0.0773	0.0770	<b>0.0869</b>	<b>0.0792</b>	<b>0.0667</b>	<b>0.0633</b>	2.31
6	4	2	3	10	Indep.	<b>0.0312</b>	0.0924	0.2521	0.4061	0.6382	0.7159	1.69
					Ctree	0.0352	<b>0.0801</b>	0.1110	0.1176	0.1036	0.0844	2.88
					VAEAC	0.0829	0.0900	<b>0.0821</b>	<b>0.0800</b>	<b>0.0704</b>	<b>0.0559</b>	2.87

**Table 3:** Table of average MAE for the mixed data simulations outlined in Table 2 for various dependencies  $\rho$  using  $K = 250$  Monte Carlo samples. In both settings, **VAEAC** performs best for correlated data, with **ctree** a clear second. The last column reports the average CPU time in minutes needed to generate the estimated Shapley values for  $N_{\text{test}} = 500$  test observations, that is, one repetition for one value of  $\rho$ .

results for both experiments. That is, the **independence** approach is best for independent data ( $\rho = 0$ ). For  $\rho = 0.1$ , **ctree** is the best approach, closely followed by the **VAEAC** and **independence** approaches. For moderate to strong dependence ( $\rho \geq 0.3$ ) **VAEAC** is the best approach and often with a distinct margin. The **independence** approach performs increasingly worse for increasing dependence, which demonstrates the necessity of methods that can handle dependent data, such as the proposed **VAEAC** approach.

The last column of Table 3 displays the average CPU time needed to explain  $N_{\text{test}} = 500$  test observations. In both experiments, the **independence** approach is the fastest. For the smallest experiment with  $M = 4$ , the **ctree** approach is computationally faster than **VAEAC**, but they are nearly identical for the larger experiment with  $M = 6$ -dimensional mixed data.

## 5 Application on Real Data Example

In this section, we explain predictions made by a random forest model fitted to the classical Abalone data set with mixed features. The data set originates from a study by the Tasmanian Aquaculture and Fisheries Institute (Nash et al. 1994). It has been used in several XAI papers (Aas, Nagler, et al. 2021; Frye et al. 2021) and other machine-learning studies (Mohammed et al. 2020; Sahin et al. 2018; Smith et al. 2018) as it is freely available from the UCI Machine Learning Repository <http://archive.ics.uci.edu/ml/datasets/Abalone>.

An abalone is an edible marine snail, and the harvest of abalones is subject to quotas that are partly based on the age distribution. It is a time-consuming task to determine the age of abalones, as one has to cut the shell through its cone, stain it, and manually count the number of rings through a microscope. The goal is therefore to predict the age of abalones based on other easier obtainable physical measurements. The Abalone data set consists of 4177 samples with 9 features each: **Rings** (+1.5 gives the age in years), **Length** (longest shell measurement), **Diameter** (perpendicular to length), **Height** (with meat in shell), **WholeWeight** (whole abalone), **ShuckedWeight** (weight of meat), **VisceraWeight** (gut-weight after bleeding), **ShellWeight** (after being dried), and **Sex** (female, infant, male). The distances are given in millimeters and weights in grams. **Rings** is an integer, **Sex** is categorical with 3 categories, and the rest of the features are continuous. Hence, **VAEAC** will be a suitable method for this mixed-data set, in addition to the other methods used in Section 4.3.

An overview of the Abalone data set can be seen in Figure 2, where we show the pairwise scatter plots, marginal density functions, and pairwise Pearson correlation coefficients (for

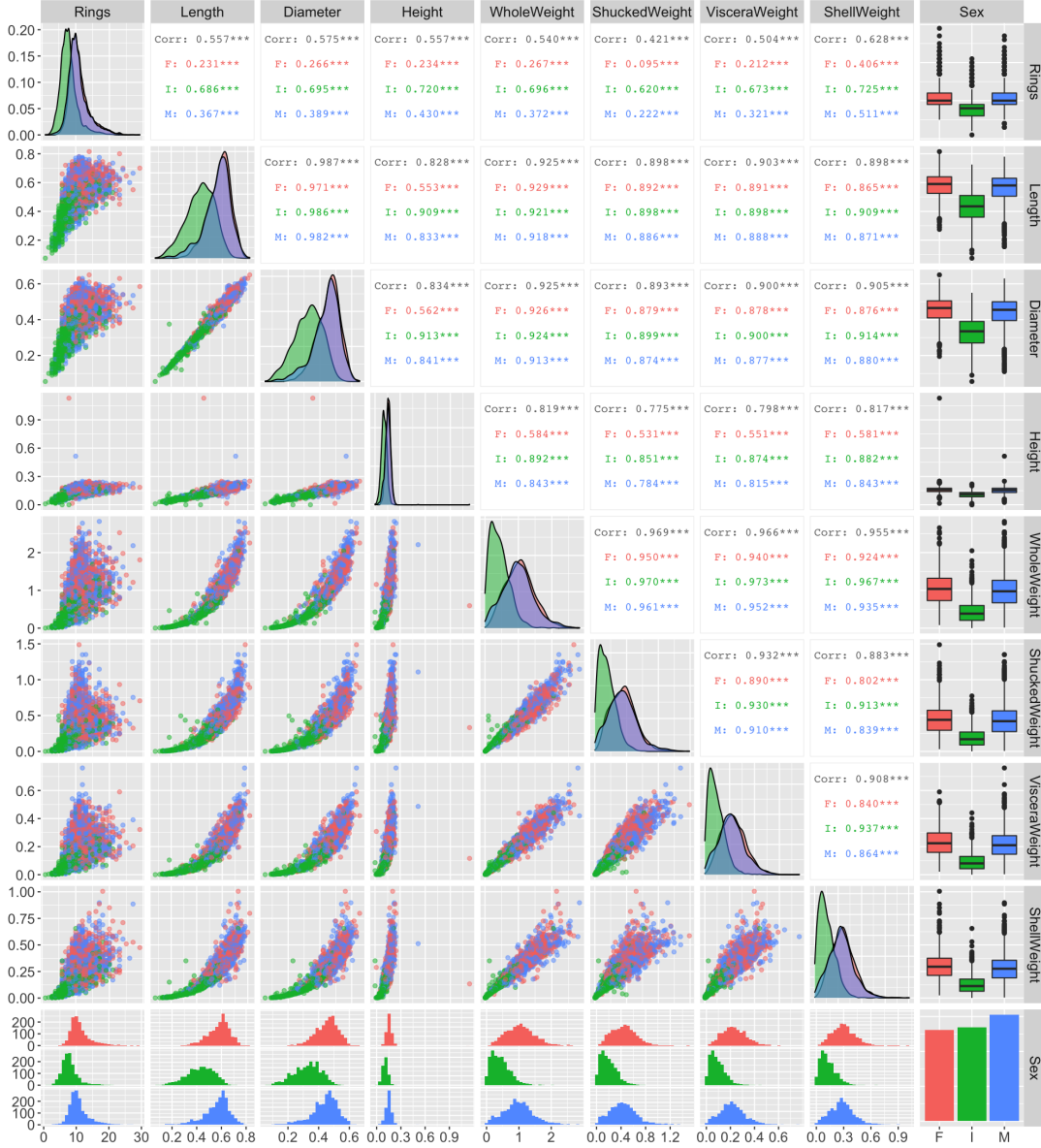


**Figure 2:** Pairwise scatter plots, marginal density functions, and pairwise correlation coefficients for the response variable **Rings** and the features of the Abalone data set. The figure is grouped by **Sex**, where the females are red, infants are green, and males are blue. The data is highly correlated and display a clear distinction between infants and females/males.

continuous features). There is a clear non-linearity and heteroscedasticity among the pairs of features, and there is significant pairwise correlation between the features. All continuous features have a pairwise correlation above 0.775, or 0.531 when grouped by **Sex**.

Aas, Nagler, et al. (2021) also used the Abalone data set when demonstrating their method for estimating Shapley values. However, their method lacks support for categorical features, hence, they discarded the categorical feature **Sex**. We consider this to be a critical

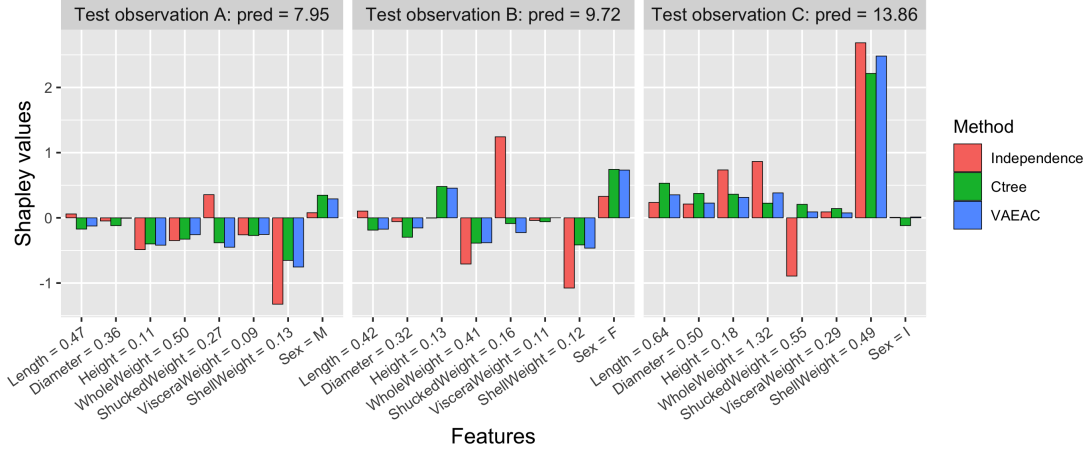


**Figure 3:** Shapley values for 3 test observations, where the predicted response is included in the header. The VAEAC and ctree approaches yield similar estimates, while the independence approach often differ in both magnitude and direction.

methodological limitation, as we will show that **Sex** is the most important feature for some test observations. This is not surprising, as Figure 2 displays a clear distinction between infants and females/males. Hence, it is important to include **Sex** in the prediction problem.

We treat the **Rings/age** prediction as a regression problem. We split the data set at random into a test and training set consisting of 100 and 4077 samples, respectively. We use a random forest model as it can detect any potential non-linear relationships between the response and the features. The model was fitted to the training data using the R-package **ranger** (Wright and Ziegler 2017) with 500 trees and default parameter settings.

Figure 3 shows the estimated Shapley values for three test observations, based on the **independence**, **ctree**, and **VAEAC** approaches. Recall from Section 2.2 that the Shapley values for a test observation  $\mathbf{x}^*$  explain the difference between the prediction  $f(\mathbf{x}^*)$  and the global average prediction  $\phi_0 = \mathbb{E}[f(\mathbf{x})]$ . We estimate  $\phi_0$  by the mean of the response in the training set, which is  $\phi_0 = 9.93$  in our training set. The three displayed test observations are chosen such that their predicted responses are, respectively, below, similar to, and above  $\phi_0$ . Moreover, they have different values of the feature **Sex**. This entails that observation A has mostly negative Shapley values, while observation B has a mixture of positive and negative Shapley values, and observation C has primarily positive Shapley values.

The Shapley values based on the **ctree** and **VAEAC** approaches are comparable. They both give **Sex** the largest absolute Shapley value for test observation B, that is, the categorical feature is an important feature to explain the predictive model. The importance of **Sex** is similar to that of other features for test observation A, while it is negligible for test observation C. For test observations A and C, **ShellWeight** is the most important feature.

The **independence** approach often yields distinctly different results than the **ctree** and **VAEAC** methods, both in magnitude and direction. We do not trust the Shapley values of the **independence** approach, as there is strong feature dependence in our data. Based on **independence**'s poor performance on dependent data in the simulations studies, we strongly believe the associated explanations to be incorrect and that they should be discarded. In the next section, we further justify the use of the **ctree** and **VAEAC** approaches.

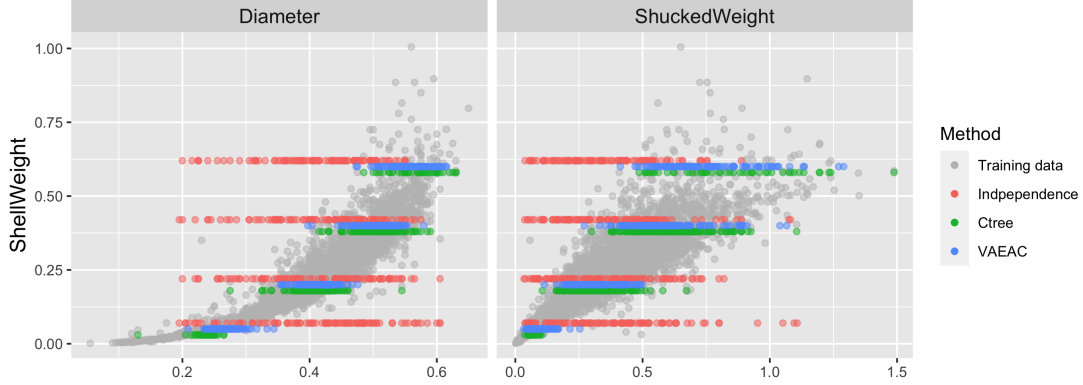


**Figure 4:** Sampling from the estimated conditional distributions using the **independence** (red), **ctree** (green), and **VAEAC** (blue) approaches. The gray dots are the training data. The samples are generated conditioned on  $\text{ShellWeight} \in \{0.05, 0.2, 0.4, 0.6\}$ . Note that the red and green dots have been slightly displaced vertically to improve visibility of the figure. The **ctree** and **VAEAC** approaches yield on-distribution data, while the **independence** method generates samples off-distribution.

## 5.1 Evaluation

For all approaches treated in this paper, the Shapley value in (1) is a weighted sum of differences  $v(\mathcal{S} \cup \{j\}) - v(\mathcal{S})$  over possible subsets  $\mathcal{S}$ . However, the approaches differ in how  $v(\mathcal{S})$ , or more specifically, the conditional distribution  $p(\mathbf{x}_{\bar{\mathcal{S}}} | \mathbf{x}_{\mathcal{S}} = \mathbf{x}_{\mathcal{S}}^*)$ , is estimated. We now illustrate that the generated conditional samples using the **VAEAC** and **ctree** approaches are more representative than the samples of the **independence** method. Thus, it is likely that the estimated Shapley values using the former two methods are more accurate for the Abalone example.

Since there are  $2^M = 2^8 = 256$  conditional distributions involved in the Shapley formula, it is impossible to show all here. However, we have included some examples to illustrate that the **VAEAC** and **ctree** approaches give more correct approximations to the true conditional distributions than the **independence** approach. Figure 4 shows pairplots of **ShellWeight** against both **Diameter** and **ShuckedWeight**, where the grey dots are the training data. The red, green, and blue dots are generated samples from the estimated conditional distribution of the variable on the x-axis given  $\text{ShellWeight} \in \{0.05, 0.2, 0.4, 0.6\}$ , using the **independence**, **ctree**, and **VAEAC** approaches, respectively.

The **independence** approach generates unrealistic samples far outside the range of observed values in the training data, in contrast to the **VAEAC** and **ctree** methods. It is well known that evaluation of predictive machine learning models far from the domain at which they have been trained, can lead to spurious predictions. Thus, it is important that the explanation methods are evaluating the predictive model at appropriate feature combinations.

## 6 Conclusion

Shapley values originated in cooperative game theory and have a solid theoretical foundation. It gained momentum as a model-agnostic explanation framework for explaining individual predictions following the work of Lundberg and Lee (2017). However, their work relied on the assumption of independent features. Thus, their methodology may lead to incorrect



explanations when the features are dependent, which is often the case for real-world data. There have been several proposed methods for appropriately modeling the dependence between the features, but this is computationally expensive as the number of feature combinations to model grows exponentially with the number of features.

This paper aimed to introduce the variational autoencoder with arbitrary condition **VAEAC** (Ivanov et al. 2019) as a tool to estimate the conditional expectation in the Shapley value explanation framework. The **VAEAC** method models the dependence structure between all feature combinations simultaneously using a single variational autoencoder. This is in contrast to the state-of-the-art dependence aware methods available in the R-package **shapr** (Sellereite and Jullum 2019), which fits a new model to each feature combination. Furthermore, **VAEAC** supports a mixture of continuous and categorical features. The **ctree** approach (Redelmeier et al. 2020) is the only other method that directly supports dependent mixed features. The other methods could be extended to support categorical features by using one-hot encoding, but this is in general infeasible as it drastically increases the computational complexity.

Through a series of simulation studies, we have demonstrated that the **VAEAC** approach outperforms or matches the state-of-the-art dependence aware approaches, even for very small training sets. In addition to yielding more accurate Shapley values than the other methods, **VAEAC** was also computationally faster than most of the other methods, in our simulations. However, the computation times are generally large in the Shapley value explanation framework as we need to model an exponential amount of feature dependencies. This can be mitigated substantially by parallelizing computations and/or using the approximated weighted least squares method proposed by Lundberg and Lee (2017).

The **VAEAC** approach was used to explain predictions made by a random forest model designed to predict the age of an abalone (marine snail). In this case, the true Shapley values are unknown, but we saw a strong coherency between the explanations from the **VAEAC** and **ctree** approaches. The **independence** approach gave different Shapley values both in direction and magnitude. We provided results which indicated that the former two approaches provide more sensible Shapley value estimates than the latter.

In the current implementation of **VAEAC**, we use the Gaussian distribution to model the continuous features. This can generate inappropriate values if the feature values are, for example, strictly positive or restricted to an interval  $(a, b)$ . In such settings **VAEAC** can generate negative samples or samples outside the interval, respectively. A naive approach is to set the negative values to zero and the values outside the interval to the nearest endpoint value. However, a better approach would be to transform the data to an unbounded form before using the **VAEAC** approach. That is, strictly positive values can be log-transformed, while interval values can first be mapped to  $(0, 1)$  and then further to the full real line by, for example, the logit function. A more complicated, but certainly interesting, approach is to replace the Gaussian distribution in the decoder with a distribution which has support on the same range as the features, like the gamma distribution for strictly positive values and the beta distribution for values in  $(0, 1)$ .

## Acknowledgments

This work was supported by The Norwegian Research Council 237718 through the Big Insight Center for research-driven innovation. In addition, the authors want to thank Annabelle Redelmeier for advice on the mixed data simulation study.

## Appendix

We start the appendix by giving a brief description of the alternative approaches to **VAEAC** in Appendix A. In Appendix B, we give the full derivation of the variational lower bound. The implementation details of **VAEAC** are discussed in Appendix C. In Appendix D, we conduct a simulation study with only categorical features. The data generating process of the different simulations studies are elaborated in Appendix E. Finally, in Appendix F, we experiment with different number of Monte Carlo samples.

### A Alternative Approaches

In this section, we give a short description of the other approaches available in the R-package **shapr** (Sellereite and Jullum 2019), that is, the **independence**, **empirical**, **Gaussian**, **copula**, and **ctree** approaches. We use the default hyperparameters implemented in the **shapr**-package when using these methods.

Method	Citation	Description
<b>Independence</b>	Lundberg and Lee (2017)	Assume the features are independent. Estimate (2) by (3) where $\mathbf{x}_{\mathcal{S}}^{(k)}$ are sub-samples from the training data.
<b>Empirical</b>	Aas, Jullum, et al. (2021)	Calculate the Mahalanobis distance between the observation being explained and every training instance. Use this distance to calculate a weight for each training instance using $\eta = 1$ . Approximate (2) using a function of these weights.
<b>Gaussian</b>	Aas, Jullum, et al. (2021)	Assume the features are jointly Gaussian. Sample $K$ times from the corresponding conditional distribution. Estimate (2) with (3) using these samples.
<b>Copula</b>	Aas, Jullum, et al. (2021)	Assume the dependence structure of the features can be approximated by a Gaussian copula. Sample $K$ times from the corresponding conditional distribution. Estimate (2) with (3) using these samples.
<b>Ctree</b>	Redelmeier et al. (2020)	Fit conditional inference trees for each coalition. Sample $K$ times from the corresponding conditional distribution (with replacements). Estimate (2) with (3) using these samples.

**Table 4:** A short description of the approaches used to estimate (2) in the simulation studies.

## B Variational Lower Bound for VAEAC

Here we give the full derivation of the variational lower bound in (6):

$$\begin{aligned}
\log p_{\psi, \theta}(\mathbf{x}_{\bar{\mathcal{S}}} | \mathbf{x}_{\mathcal{S}}, \bar{\mathcal{S}}) &= \int p_{\phi}(\mathbf{z} | \mathbf{x}, \bar{\mathcal{S}}) \log p_{\psi, \theta}(\mathbf{x}_{\bar{\mathcal{S}}} | \mathbf{x}_{\mathcal{S}}, \bar{\mathcal{S}}) d\mathbf{z} \\
&= \mathbb{E}_{p_{\phi}(\mathbf{z} | \mathbf{x}, \bar{\mathcal{S}})} [\log p_{\psi, \theta}(\mathbf{x}_{\bar{\mathcal{S}}} | \mathbf{x}_{\mathcal{S}}, \bar{\mathcal{S}})] \\
&= \mathbb{E}_{p_{\phi}(\mathbf{z} | \mathbf{x}, \bar{\mathcal{S}})} \left[ \log \frac{p_{\psi, \theta}(\mathbf{x}_{\bar{\mathcal{S}}}, \mathbf{z} | \mathbf{x}_{\mathcal{S}}, \bar{\mathcal{S}})}{p_{\psi, \theta}(\mathbf{z} | \underbrace{\mathbf{x}_{\mathcal{S}}, \mathbf{x}_{\bar{\mathcal{S}}}}_{\mathbf{x}}, \bar{\mathcal{S}})} \right] \\
&= \mathbb{E}_{p_{\phi}(\mathbf{z} | \mathbf{x}, \bar{\mathcal{S}})} \left[ \log \left\{ \frac{p_{\psi, \theta}(\mathbf{x}_{\bar{\mathcal{S}}}, \mathbf{z} | \mathbf{x}_{\mathcal{S}}, \bar{\mathcal{S}})}{p_{\phi}(\mathbf{z} | \mathbf{x}, \bar{\mathcal{S}})} \frac{p_{\phi}(\mathbf{z} | \mathbf{x}, \bar{\mathcal{S}})}{p_{\psi, \theta}(\mathbf{z} | \mathbf{x}, \bar{\mathcal{S}})} \right\} \right] \\
&= \mathbb{E}_{p_{\phi}(\mathbf{z} | \mathbf{x}, \bar{\mathcal{S}})} \left[ \log \frac{p_{\psi, \theta}(\mathbf{x}_{\bar{\mathcal{S}}}, \mathbf{z} | \mathbf{x}_{\mathcal{S}}, \bar{\mathcal{S}})}{p_{\phi}(\mathbf{z} | \mathbf{x}, \bar{\mathcal{S}})} \right] + \mathbb{E}_{p_{\phi}(\mathbf{z} | \mathbf{x}, \bar{\mathcal{S}})} \left[ \log \frac{p_{\phi}(\mathbf{z} | \mathbf{x}, \bar{\mathcal{S}})}{p_{\psi, \theta}(\mathbf{z} | \mathbf{x}, \bar{\mathcal{S}})} \right] \\
&= \mathbb{E}_{p_{\phi}(\mathbf{z} | \mathbf{x}, \bar{\mathcal{S}})} \left[ \log \frac{p_{\psi, \theta}(\mathbf{x}_{\bar{\mathcal{S}}}, \mathbf{z} | \mathbf{x}_{\mathcal{S}}, \bar{\mathcal{S}})}{p_{\phi}(\mathbf{z} | \mathbf{x}, \bar{\mathcal{S}})} \right] + \underbrace{D_{\text{KL}}(p_{\phi}(\mathbf{z} | \mathbf{x}, \bar{\mathcal{S}}) \parallel p_{\psi, \theta}(\mathbf{z} | \mathbf{x}, \bar{\mathcal{S}}))}_{\geq 0} \\
&\geq \mathbb{E}_{p_{\phi}(\mathbf{z} | \mathbf{x}, \bar{\mathcal{S}})} \left[ \log \frac{p_{\psi, \theta}(\mathbf{x}_{\bar{\mathcal{S}}}, \mathbf{z} | \mathbf{x}_{\mathcal{S}}, \bar{\mathcal{S}})}{p_{\phi}(\mathbf{z} | \mathbf{x}, \bar{\mathcal{S}})} \right] \\
&= \mathbb{E}_{p_{\phi}(\mathbf{z} | \mathbf{x}, \bar{\mathcal{S}})} \left[ \log \frac{p_{\theta}(\mathbf{x}_{\bar{\mathcal{S}}} | \mathbf{z}, \mathbf{x}_{\mathcal{S}}, \bar{\mathcal{S}}) p_{\psi}(\mathbf{z} | \mathbf{x}_{\mathcal{S}}, \bar{\mathcal{S}})}{p_{\phi}(\mathbf{z} | \mathbf{x}, \bar{\mathcal{S}})} \right] \\
&= \mathbb{E}_{p_{\phi}(\mathbf{z} | \mathbf{x}, \bar{\mathcal{S}})} [\log p_{\theta}(\mathbf{x}_{\bar{\mathcal{S}}} | \mathbf{z}, \mathbf{x}_{\mathcal{S}}, \bar{\mathcal{S}})] + \mathbb{E}_{p_{\phi}(\mathbf{z} | \mathbf{x}, \bar{\mathcal{S}})} \left[ \log \frac{p_{\psi}(\mathbf{z} | \mathbf{x}_{\mathcal{S}}, \bar{\mathcal{S}})}{p_{\phi}(\mathbf{z} | \mathbf{x}, \bar{\mathcal{S}})} \right] \\
&= \mathbb{E}_{p_{\phi}(\mathbf{z} | \mathbf{x}, \bar{\mathcal{S}})} [\log p_{\theta}(\mathbf{x}_{\bar{\mathcal{S}}} | \mathbf{z}, \mathbf{x}_{\mathcal{S}}, \bar{\mathcal{S}})] - \mathbb{E}_{p_{\phi}(\mathbf{z} | \mathbf{x}, \bar{\mathcal{S}})} \left[ \log \frac{p_{\phi}(\mathbf{z} | \mathbf{x}, \bar{\mathcal{S}})}{p_{\psi}(\mathbf{z} | \mathbf{x}_{\mathcal{S}}, \bar{\mathcal{S}})} \right] \\
&= \mathbb{E}_{p_{\phi}(\mathbf{z} | \mathbf{x}, \bar{\mathcal{S}})} [\log p_{\theta}(\mathbf{x}_{\bar{\mathcal{S}}} | \mathbf{z}, \mathbf{x}_{\mathcal{S}}, \bar{\mathcal{S}})] - D_{\text{KL}}(p_{\phi}(\mathbf{z} | \mathbf{x}, \bar{\mathcal{S}}) \parallel p_{\psi}(\mathbf{z} | \mathbf{x}_{\mathcal{S}}, \bar{\mathcal{S}})) \\
&= \mathcal{L}_{\text{VAEAC}}(\mathbf{x}, \bar{\mathcal{S}} | \theta, \psi, \phi).
\end{aligned}$$

## C Implementation Details of VAEAC

In this section, we describe different implementation details, masking schemes, and possible implementation improvements for the VAEAC approach.

### C.1 Fixed-length Input and Output

In Section 3, we used a simplified representation to focus the spotlight on the essential aspects of the VAEAC approach. We now provide the full implementation details.

The VAEAC method is implemented in the auto-grad framework PyTorch (Paszke et al. 2019). In the implementation, we need to take into consideration that the number of unobserved features  $|\bar{\mathcal{S}}|$  varies depending on the coalition  $\mathcal{S}$ . Hence, the input of the encoder and masked encoder will be of varying length, which is inconsistent with NNs' assumption of fixed-length input. Figure 5 is an extended version of Figure 1 where we introduce a zeroth layer  $L^*$  in the encoder and masked encoder which enforces a fixed-length input to the first layer  $L_1$  of the NNs. To ensure masks  $\bar{\mathcal{S}}$  of equal length, we introduce  $I(\bar{\mathcal{S}}) = \{\mathbb{I}(j \in \bar{\mathcal{S}}) : j = 1, \dots, M\} \in \{0, 1\}^M$ , which is an  $M$ -dimensional binary vector where the  $j$ th element  $I(\bar{\mathcal{S}})_j$  is 1 if the  $j$ th feature

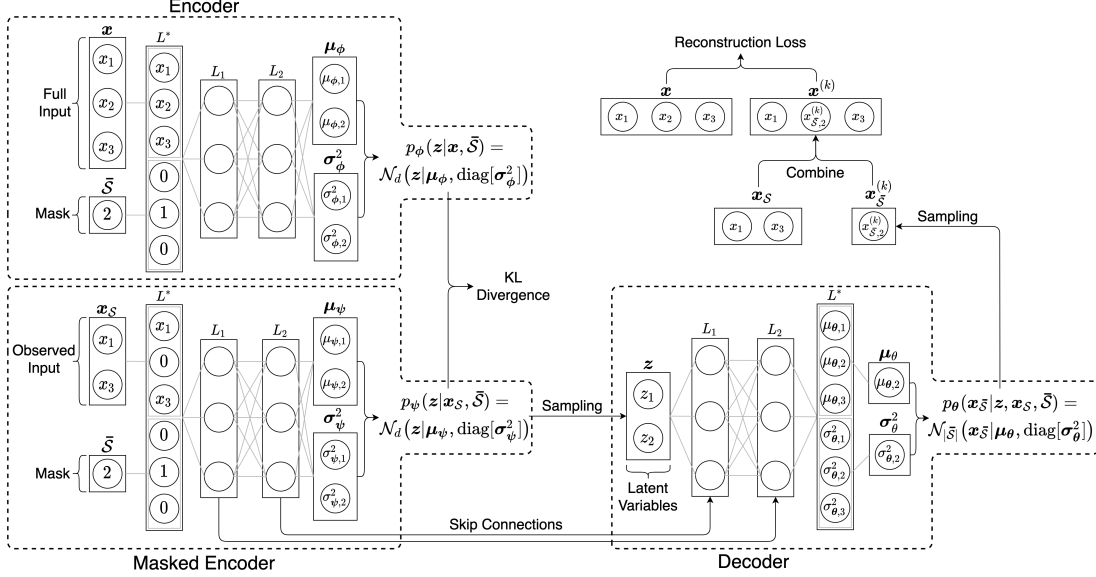


**Figure 5:** An extended version of Figure 1 where we include the fixed-length implementation details introduced in Appendix C.1.

is unobserved and 0 otherwise. For a fixed-length observed feature vector  $\mathbf{x}_S$ , we define  $\tilde{\mathbf{x}}_S = \mathbf{x} \circ I(\mathcal{S})$ , where  $\circ$  is the element-wise product. Similarly, the decoder also has a fixed-length output. Thus, we also introduce a last layer  $L^*$  in the decoder which extracts the relevant values of  $\mu_\theta$  and  $\sigma_\theta^2$  for the mask  $\tilde{\mathcal{S}}$ .

We now elaborate the example given in Section 3.2 with  $\mathbf{x} = \{x_1, x_2, x_3\}$ ,  $\mathcal{S} = \{1, 3\}$  and  $\tilde{\mathcal{S}} = \{2\}$ . The observed and unobserved feature vectors are  $\mathbf{x}_S = \{x_1, x_3\}$  and  $\mathbf{x}_{\tilde{\mathcal{S}}} = \{x_2\}$ , respectively. The associated fixed-length versions computed in layer  $L^*$  are  $I(\tilde{\mathcal{S}}) = \{0, 1, 0\}$  and  $\tilde{\mathbf{x}}_S = \{x_1, x_2, x_3\} \circ \{1, 0, 1\} = \{x_1, 0, x_3\}$ . Note that VAEAC does not have issues with differentiating actual zeros from zeros induced by the fixed-length transformation as it has access to  $I(\tilde{\mathcal{S}})$ . We consider these implementation details to be a part of the NN architecture, hence, the tilde-notation and the  $I$  function are not included in the mathematical derivations. The final complete sample is therefore  $\mathbf{x}^{(k)} = \mathbf{x}_{\tilde{\mathcal{S}}}^{(k)} \circ I(\tilde{\mathcal{S}}) + \mathbf{x}_S \circ I(\mathcal{S})$ .

## C.2 Hyperparameters

There are several hyperparameters to set before training a VAEAC, both architecturally and training-wise. The NNs of the encoder, masked encoder, and decoder can be of different size, but throughout the paper we use shared parameters and set `depth` = 3, `width` = 32, `d` = `latent_dim` = 8 based on experience. This gives a total of 18724 model parameters, which are tuned using the Adam optimization algorithm (Kingma and Ba 2015) with learning rate `lr` = 0.001. Smaller networks can be used, but we found them to perform sub-optimal for the simulation studies in this paper.

We use the same values for the hyperparameters  $\sigma_\mu$  and  $\sigma_\sigma$  of the prior in latent space as Ivanov et al. (2019), that is,  $10^4$  for both of them. This value correspond to a very weak, almost disappearing, regularization. That is, the distribution is close to uniform near zero and does not affect the learning process significantly. The activation function used is LeakyReLU, with the default parameters set in the PyTorch implementation. We use `batch_size` = 64

and generate  $K = 250$  Monte Carlo samples from each conditional distribution for each test observation. The masking scheme  $p(\bar{\mathcal{S}})$  is set to have equal probability for all coalitions  $\bar{\mathcal{S}}$ , as we did not find more intricate masking schemes to perform better, see Appendix C.3.

In all simulation studies, we let the number of epochs be `epochs` = 200. We use the VAEAC model at the epoch with the lowest *importance sampling* estimate, denoted by IWAE (Sohn et al. 2015). The IWAE estimates the log-likelihood by

$$\text{IWAE} = \log \frac{1}{V} \sum_{i=1}^V \frac{p_{\psi}(z_i | \mathbf{x}_S, \bar{\mathcal{S}}) p_{\theta}(\mathbf{x}_{\bar{\mathcal{S}}} | z_i, \mathbf{x}_S, \bar{\mathcal{S}})}{p_{\phi}(z_i | \mathbf{x}_S, \bar{\mathcal{S}})} \approx \log p_{\psi, \theta}(\mathbf{x}_{\bar{\mathcal{S}}} | \mathbf{x}_S, \bar{\mathcal{S}}), \quad (12)$$

where  $V$  is the number of IWAE validation samples  $z_i \sim p_{\phi}(z_i | \mathbf{x}_S, \bar{\mathcal{S}})$  generated for each  $\mathbf{x}_S$ . We set  $V = 40$ . The IWAE is computed on a hold out validation set which is set to be 25% of the training data. That is, if  $N_{\text{train}} = 100$ , we actually only use 75 observations to train the VAEAC model and the rest to validate the trained model.

To stabilize the results, we initiate 15 VAEAC models, let them run for 5 epochs, and then only continue training the VAEAC with lowest VLB. This is to reduce the effect of the randomly initiated model parameters, which can put VAEAC in a sub-optimal part of the parameter space which it cannot escape. One could also use other types of adaptive learning rates to solve this problem, see Goodfellow, Bengio, et al. (2016, Ch. 8).

### C.3 Masking Scheme

Throughout the simulations studies, we used the uniform masking scheme  $p(\bar{\mathcal{S}}) = 2^{-M}$ . That is, each mask is of equal importance, which can be modeled as a feature-wise Bernoulli(0.5). As  $p(\bar{\mathcal{S}})$  has full support over the set of all subsets of  $\mathcal{M}$ ,  $p_{\psi, \theta}(\mathbf{x}_{\bar{\mathcal{S}}} | \mathbf{x}_S, \bar{\mathcal{S}})$  can evaluate arbitrary conditioning. However, we can specify  $p(\bar{\mathcal{S}})$  such that VAEAC concentrates more of its estimation efforts on certain coalitions/masks. As the coalitions are weighted differently in the Shapley value formula (1), we investigated if different masking schemes could improve the precision of the estimated Shapley values. This was inspired by the work of Gautam et al. (2020) on different masking schemes for universal marginalizers (Douglas et al. 2017).

We considered four additional versions of  $p(\bar{\mathcal{S}})$ , which all have full support over the set of all subsets of  $\mathcal{M}$ : 1)  $p(\bar{\mathcal{S}}) \propto \binom{M}{|\bar{\mathcal{S}}|}$  (i.e., the binomial coefficient), 2)  $p(\bar{\mathcal{S}}) \propto 1/\binom{M}{|\bar{\mathcal{S}}|}$ , 3) Shapley kernel weights derived in Lundberg and Lee (2017), and 4) Shapley kernel weights scaled by  $1/\binom{M}{|\bar{\mathcal{S}}|}$ . Here  $|\bar{\mathcal{S}}|$  denotes the number of unobserved features and we scale all schemes such that they sum to 1. We found no significant improvement over the original uniform masking scheme and there was no systematic tendency in which scheme performed the best. These results are reassuring as they imply that a properly fitted VAEAC model with a masking scheme with full support can conduct arbitrary conditioning. That is, VAEAC extracts all informative conditional information in the data for *all* coalitions even when focusing more on certain coalitions.

### C.4 Improvements in Implementation

The current implementation of VAEAC can be improved in several ways. First, we have used a conservative number of epochs during training, but the IWAE (12) often stabilizes before the reaching the last epoch. Hence, the fitting time of VAEAC could be reduced by applying some type of early stopping regime if no improvement is seen in the IWAE over several epochs. Second, the sampling process of VAEAC is not parallelized. However, as the test observations are independent, the associated conditional samples could be generated simultaneously on separate CPUs.

$M$	$L$	$N_{\text{test}}$	Categorical cut-off values
3	3	27	$(-\infty, 0, 1, \infty)$
3	4	64	$(-\infty, -0.5, 0, 1, \infty)$
4	3	81	$(-\infty, 0, 1, \infty)$
5	6	2000	$(-\infty, -1.5, -1, 0, 0.5, 1, \infty)$
7	4	2000	$(-\infty, -0.5, 0.5, 1, \infty)$
10	3	2000	$(-\infty, -0.5, 1, \infty)$

**Table 5:** Outline of the setup of the categorical simulation studies in Appendix D. The fourth column describes the cut-off values between the different categories.

## D Simulation Study: Categorical Data

The categorical simulation study follows the setup of Redelmeier et al. (2020). Their results are based on a single run, which can lead to incorrect conclusions as the results vary significantly between each repetition, hence, we conduct repeated simulations. Similarly to the mixed data studies in Section 4.3, we compare the VAEAC approach with the **independence** and **ctree** methods.

Let  $\{\mathbf{x}^{(i)}\}_{i=1, \dots, N_{\text{test}}}$  be the set of all unique  $M$ -dimensional categorical observations where each feature has  $L$  categories. Thus,  $N_{\text{test}} = L^M$ , which is manageable for small dimensional settings. We replace  $N_{\text{test}}$  in the denominator of MAE (9) by  $p(\mathbf{x}^{(i)})$ , the corresponding probability mass function, and move it inside the summation. In larger dimensional settings, we use a subset of the  $N_{\text{test}} = 2000$  most likely feature combinations and scale the probabilities such that they sum to 1 over those combinations.

The categorical data generating process and related Shapley value computations are elaborated in Appendix E.3. The main point there is that the categorical data is generated by sampling from a multivariate Gaussian  $\mathcal{N}_M(\boldsymbol{\mu}, \Sigma_\rho)$  before categorizing each of the  $M$  variables into  $L$  categories at certain cut-off-values, defined in Table 5. The covariance matrix  $\Sigma_\rho$ , which reflects the feature dependence, is 1 on the diagonal and  $\rho$  off-diagonal.

We consider six different setups which are described in Table 5. We use  $N_{\text{train}} = 1000$  training observations to fit the predictive model, while  $\boldsymbol{\mu} = \mathbf{0}$  and  $\rho \in \{0.0, 0.1, 0.3, 0.5, 0.8, 0.9\}$ . The response is generated according to

$$y_i = \alpha + \sum_{j=1}^M \sum_{l=1}^L \beta_{jl} \mathbb{I}(x_{ij} = l) + \epsilon_i, \quad (13)$$

where  $x_{ij}$  is the  $j$ th feature of the  $i$ th training observation and  $\epsilon_i \sim \mathcal{N}(0, 0.1^2)$ , for  $i = 1, \dots, N_{\text{train}}$ . The parameters  $\alpha, \beta_{jl}$  are sampled from  $\mathcal{N}(0, 1)$ , for  $j = 1, \dots, M$  and  $l = 1, \dots, L$ . The predictive model  $f$  takes the same form as (13), but without the noise term. The model parameters are estimated using standard linear regression.

The results of the categorical experiments are shown in Table 6. For all dimensions, we see that the **independence** approach is the best for independent data ( $\rho = 0$ ). However, both **ctree** and VAEAC significantly outperform **independence** for moderate to strong correlation ( $\rho \geq 0.3$ ), which is common in real-world data. For the smaller experiments ( $M \leq 4$ ), we see that **ctree** performs better than VAEAC in most settings, except for  $\rho = 0.5$  in two of the experiments. We have no intuitive explanation for why VAEAC outperforms **ctree** for this particular correlation. For the larger experiments with moderate to strong dependence, we see that VAEAC more often outperforms **ctree** than for the smaller experiments, especially for

$M$	$L$	Rep	Method	$\overline{\text{MAE}}$ for each $\rho$					
				0.0	0.1	0.3	0.5	0.8	0.9
3	3	20	Indep.	<b>0.01696</b>	<b>0.03566</b>	0.09461	0.14875	0.25836	0.36230
			Ctree	0.02287	0.03780	<b>0.04275</b>	<b>0.03525</b>	<b>0.02981</b>	<b>0.02767</b>
			VAEAC	0.03953	0.04234	0.04825	0.04139	0.04253	0.04278
3	4	20	Indep.	<b>0.01769</b>	<b>0.03900</b>	0.10383	0.14817	0.29045	0.37327
			Ctree	0.02308	0.03931	<b>0.05290</b>	0.05117	<b>0.04853</b>	<b>0.04006</b>
			VAEAC	0.03962	0.04792	0.05326	<b>0.05014</b>	0.05084	0.05357
4	3	20	Indep.	<b>0.01817</b>	<b>0.04118</b>	0.12593	0.18220	0.26096	0.35899
			Ctree	0.02126	0.04321	<b>0.04884</b>	0.04801	<b>0.04171</b>	<b>0.03339</b>
			VAEAC	0.03871	0.04754	0.05140	<b>0.04744</b>	0.04455	0.03886
5	6	10	Indep.	<b>0.02631</b>	0.05190	0.12439	0.19075	0.32992	0.41757
			Ctree	0.02658	<b>0.04039</b>	<b>0.06359</b>	0.07430	<b>0.08410</b>	0.09798
			VAEAC	0.06196	0.07140	0.07245	<b>0.07202</b>	0.08589	<b>0.07480</b>
7	4	10	Indep.	<b>0.01893</b>	0.04490	0.12097	0.20202	0.34102	0.40046
			Ctree	0.02064	<b>0.04460</b>	0.06524	0.07061	0.07140	0.07360
			VAEAC	0.05128	0.05844	<b>0.06309</b>	<b>0.06550</b>	<b>0.06421</b>	<b>0.06465</b>
10	3	10	Indep.	<b>0.01626</b>	0.05512	0.12524	0.22603	0.40277	0.39948
			Ctree	0.01693	<b>0.04387</b>	0.05793	0.06184	<b>0.06134</b>	0.05784
			VAEAC	0.04977	0.04899	<b>0.05140</b>	<b>0.05659</b>	0.06616	<b>0.05606</b>

**Table 6:** Table presenting the average MAE for the different methods applied on the categorical data simulations with correlation  $\rho$ . The bolded numbers denote the smallest average MAE per experiment and  $\rho$ , that is, the best approach.

$M = 7$ . However, for independent data, VAEAC is outperformed by `independence` and `cree` in all experiments.

## E Data Generating Processes of Dependent Data

Here we present how the data are generated for the three types of simulation studies investigated in this article. In addition, we explain how we calculate the associated true Shapley values.

### E.1 Continuous Data

The continuous multivariate Burr distribution is chosen as its conditional distributions have known analytical expressions. This allows us to compute the true Shapley values with arbitrary precision. Other multivariate distributions with closed-form conditional distributions exist, for example, the multivariate normal (MVN) and the generalized hyperbolic (GH), which are fairly similar. Therefore, both would give an unfair advantage to the approaches that assume normal data, that is, the `Gaussian` and `copula` approaches. The Burr distribution is less similar to the MVN distribution, as it allows for heavy-tailed and skewed marginals and nonlinear dependence, which can be found in real-world data sets.

The  $M$ -dimensional Burr distribution has the density

$$p_M(\mathbf{x}) = \frac{\Gamma(\kappa + M)}{\Gamma(\kappa)} \left( \prod_{m=1}^M b_m r_m \right) \frac{\prod_{m=1}^M x_m^{b_m-1}}{\left( 1 + \sum_{m=1}^M r_m x_m^{b_m} \right)^{\kappa+M}},$$

for  $x_m > 0$  (Takahasi 1965). The  $M$ -dimensional Burr distribution has  $2M + 1$  parameters, namely,  $\kappa, b_1, \dots, b_M$ , and  $r_1, \dots, r_M$ . Furthermore, the Burr distribution is a compound Weibull distribution with the gamma distribution as compounder (Takahasi 1965), and it can also be seen as a special case of the Pareto IV distribution (Yari and Jafari 2006).

Any conditional distribution of the Burr distribution is in itself a Burr distribution (Takahasi 1965). Without loss of generality, assume that the first  $S < M$  features are the unobserved features, then the conditional density  $p(x_1, \dots, x_S | x_{S+1} = x_{S+1}^*, \dots, x_M = x_M^*)$ , where  $\mathbf{x}^*$  indicates the conditional values, is an  $S$ -dimensional Burr density. The associated parameters are then  $\tilde{\kappa}, \tilde{b}_1, \dots, \tilde{b}_S$ , and  $\tilde{r}_1, \dots, \tilde{r}_S$ , where  $\tilde{\kappa} = \kappa + M - S$ , while  $\tilde{b}_j = b_j$  and  $\tilde{r}_j = \frac{r_j}{1 + \sum_{m=S+1}^M r_m (x_m^*)^{b_m}}$ , for all  $j = 1, 2, \dots, S$ .

By drawing a large number  $K$  of observations from the true conditional distributions, we can compute the contribution function (2) with arbitrary precision. That is, for any subset  $\mathcal{S} \subseteq \mathcal{M}$ , we draw conditional observations  $\mathbf{x}_{\mathcal{S}}^{(k)}$  from  $p(\mathbf{x}_{\mathcal{S}} | \mathbf{x}_{\mathcal{S}^c} = \mathbf{x}_{\mathcal{S}^c}^*)$ , for  $k = 1, \dots, K$ . These  $K$  samples are used to estimate  $v(\mathcal{S})$  by  $\hat{v}_{\text{true}}(\mathcal{S}) = \frac{1}{K} \sum_{k=1}^K f(\mathbf{x}_{\mathcal{S}}^{(k)}, \mathbf{x}_{\mathcal{S}^c}^*)$ , which are then used in (1) to precisely compute the true Shapley values  $\phi_{\text{true}}$  in (9). We have used  $K = 10000$  Monte Carlo samples to compute the exact Shapley values.

An outline of one repetition of the simulation study for a fixed  $N_{\text{train}}$  and  $\kappa$  is given below. This is repeated 20 times and the average MAE (9) is presented in Table 1.

1. Generate simulated training data by
  - sampling  $N_{\text{train}}$  training observations from the chosen  $\text{Burr}(\kappa)$  distribution, and
  - computing the corresponding responses using (10).
2. Let the predictive model  $f(\mathbf{x})$  be an XGBoost model, and fit it to the training data. We use the R-package `xgboost` with `nrounds = 50` and otherwise default parameters.
3. Sample  $N_{\text{test}} = 100$  test observations from the chosen  $\text{Burr}(\kappa)$  distribution.
4. For all methods, possible coalitions  $\mathcal{S}$ , and test observations  $\mathbf{x}^{(i)}$ :
  - Generate  $K = 250$  samples, and compute  $\hat{v}(\mathcal{S})$  using (3).
  - This means setting `w_threshold = 1` for `empirical` in the `shapr`-package. Default parameters for the other methods.
5. For all test observations  $\mathbf{x}^*$  and methods, compute the estimated Shapley values using (1) and compute the MAE defined in (9).

## E.2 Mixed Data

We now present a shortened description of the dependent mixed data generating process and related Shapley value computations of Redelmeier et al. (2020). For simplicity, they use a linear predictive function of the form

$$f(\mathbf{x}) = \alpha + \sum_{j \in \mathcal{C}_{\text{cat}}} \sum_{l=1}^L \beta_{jl} \mathbb{I}(x_j = l) + \sum_{j \in \mathcal{C}_{\text{cont}}} \gamma_j x_j, \quad (14)$$



where  $\mathcal{C}_{\text{cat}}$  and  $\mathcal{C}_{\text{cont}}$  denote the set of categorical and continuous features, respectively,  $L$  is the number of categories for each of the categorical features, and  $\mathbb{I}(x_j = l)$  is the indicator function taking the value 1 if  $x_j = l$  and 0 otherwise. Furthermore,  $\alpha$ ,  $\beta_{jl}$  for  $j \in \mathcal{C}_{\text{cat}}$ ,  $l = 1, \dots, L$ , and  $\gamma_j$  for  $j \in \mathcal{C}_{\text{cont}}$  are the parameters of the linear model. The dimension of the model is  $M = |\mathcal{C}_{\text{cat}}| + |\mathcal{C}_{\text{cont}}|$ , where  $|\mathcal{C}_{\text{cat}}|$  and  $|\mathcal{C}_{\text{cont}}|$  denote the number of categorical and continuous features, respectively.

To generate  $M$ -dimensional dependent mixed data, we sample from an  $M$ -dimensional Gaussian distribution  $\mathcal{N}_M(\boldsymbol{\mu}, \Sigma_\rho)$ , but discretize  $|\mathcal{C}_{\text{cat}}|$  of the features into  $L$  categories each. Here  $\boldsymbol{\mu}$  is the mean and  $\Sigma_\rho$  is the covariance matrix, which reflects the feature dependence, and it is 1 on the diagonal and  $\rho$  off-diagonal. That is, we first sample a random variable

$$(\tilde{x}_1, \dots, \tilde{x}_M) \sim \mathcal{N}_M(\boldsymbol{\mu}, \Sigma_\rho),$$

and then transform the features  $\tilde{x}_j$ , for  $j \in \mathcal{C}_{\text{cat}}$ , to categorical features  $x_j$  using the following transformation:

$$x_j = l, \text{ if } v_l < \tilde{x}_j \leq v_{l+1}, \text{ for } l = 1, \dots, L \text{ and } j \in \mathcal{C}_{\text{cat}},$$

where  $v_1, \dots, v_{L+1}$  is an increasing and ordered set of cut-off values defining the categories with  $v_1 = -\infty$  and  $v_{L+1} = +\infty$ . We redo this  $N_{\text{train}}$  times to create a training data set of  $M$  dependent mixed features. The strength of the dependencies between the features is controlled by the correlation  $\rho$  specified in  $\Sigma_\rho$ . Furthermore, the actual value of  $x_j$  is irrelevant and the features are treated as non-ordered categorical features.

Computing the conditional expectation is troublesome for the mixed data setting, but the linear assumption of the predictive function in (14) simplifies the computations. As the predictive function is linear, the conditional expectation reduces to a linear combination of two types of univariate expectations. Let  $\mathcal{S}_{\text{cat}}$  and  $\bar{\mathcal{S}}_{\text{cat}}$  refer to the  $\mathcal{S}$  and  $\bar{\mathcal{S}}$  part of the categorical features  $\mathcal{C}_{\text{cat}}$ , respectively, with analogous sets  $\mathcal{S}_{\text{cont}}$  and  $\bar{\mathcal{S}}_{\text{cont}}$  for the continuous features. We can then write the desired conditional expectation as

$$\begin{aligned} \mathbb{E}[f(\mathbf{x}) | \mathbf{x}_{\mathcal{S}} = \mathbf{x}_{\mathcal{S}}^*] &= \mathbb{E} \left[ \alpha + \sum_{j \in \mathcal{C}_{\text{cat}}} \sum_{l=1}^L \beta_{jl} \mathbb{I}(x_j = l) + \sum_{j \in \mathcal{C}_{\text{cont}}} \gamma_j x_j \mid \mathbf{x}_{\mathcal{S}} = \mathbf{x}_{\mathcal{S}}^* \right] \\ &= \alpha + \sum_{j \in \mathcal{C}_{\text{cat}}} \sum_{l=1}^L \beta_{jl} \mathbb{E}[\mathbb{I}(x_j = l) | \mathbf{x}_{\mathcal{S}} = \mathbf{x}_{\mathcal{S}}^*] + \sum_{j \in \mathcal{C}_{\text{cont}}} \gamma_j \mathbb{E}[x_j | \mathbf{x}_{\mathcal{S}} = \mathbf{x}_{\mathcal{S}}^*] \\ &= \alpha + \sum_{j \in \bar{\mathcal{S}}_{\text{cat}}} \sum_{l=1}^L \beta_{jl} \mathbb{E}[\mathbb{I}(x_j = l) | \mathbf{x}_{\mathcal{S}} = \mathbf{x}_{\mathcal{S}}^*] + \sum_{j \in \mathcal{S}_{\text{cat}}} \sum_{l=1}^L \beta_{jl} \mathbb{I}(x_j^* = l) \\ &\quad + \sum_{j \in \bar{\mathcal{S}}_{\text{cont}}} \gamma_j \mathbb{E}[x_j | \mathbf{x}_{\mathcal{S}} = \mathbf{x}_{\mathcal{S}}^*] + \sum_{j \in \mathcal{S}_{\text{cont}}} \gamma_j x_j^*. \end{aligned}$$

To calculate the two conditional expectations, we use results from Arellano-Valle et al. (2006) on Gaussian selection distributions in addition to basic probability theory and numerical integration. Specifically, the conditional expectation for the continuous features takes the form

$$\mathbb{E}[x_j | \mathbf{x}_{\mathcal{S}} = \mathbf{x}_{\mathcal{S}}^*] = \int_{-\infty}^{\infty} x p(x_j = x | \mathbf{x}_{\mathcal{S}} = \mathbf{x}_{\mathcal{S}}^*) dx = \int_{-\infty}^{\infty} x p(x) \frac{p(\mathbf{x}_{\mathcal{S}} = \mathbf{x}_{\mathcal{S}}^* | x_j = x)}{p(\mathbf{x}_{\mathcal{S}})} dx, \quad (15)$$

where  $p(x)$  denotes the density of the standard Gaussian distribution,  $p(\mathbf{x}_{\mathcal{S}} = \mathbf{x}_{\mathcal{S}}^* | x_j = x)$  is the conditional distribution of  $\mathbf{x}_{\mathcal{S}}$  given  $x_j = x$ , and  $p(\mathbf{x}_{\mathcal{S}})$  is the marginal distribution of  $\mathbf{x}_{\mathcal{S}}$ . The

latter two are both Gaussian and can be evaluated at the specific vector  $\mathbf{x}_S^*$  using the R-package `mvtnorm`, see Genz and Bretz (2009). The integral is solved using numerical integration.

For the conditional expectation of the categorical features, recall that  $x_j = l$  corresponds to the original Gaussian variable  $\tilde{x}_j$  falling into the interval  $(v_l, v_{l+1}]$ . Thus, the conditional expectation takes the form

$$\mathbb{E}[\mathbb{I}(x_j = l) | \mathbf{x}_S = \mathbf{x}_S^*] = P(v_l < \tilde{x}_j \leq v_{l+1} | \mathbf{x}_S) = \int_{v_l}^{v_{l+1}} p(x) \frac{p(\mathbf{x}_S = \mathbf{x}_S^* | x_j = x)}{p(\mathbf{x}_S)} dx,$$

which can be evaluated similarly to (15) and solved with numerical integration. Once we have computed the necessary conditional expectations for each of the  $2^M$  feature subsets  $\mathcal{S}$ , we compute the Shapley values using (1). This is done for both the mixed and categorical data simulation studies.

### E.3 Categorical Data

The dependent categorical data is generated similarly to the mixed data in the previous section, except that  $|\mathcal{C}_{\text{cat}}| = M$ . That is, we discretize all the  $M$  features into  $L$  categories.

To calculate the true Shapley values  $\phi_{j, \text{true}}(\mathbf{x}^{(i)})$ , for  $j = 1, \dots, M$  and  $i = 1, \dots, N_{\text{test}}$ , we need the true conditional expectation for all feature subsets  $\mathcal{S}$ . When all the features are categorical, the conditional expectation can be written as

$$\mathbb{E}[f(\mathbf{x}) | \mathbf{x}_S = \mathbf{x}_S^*] = \sum_{\mathbf{x}_{\bar{S}} \in \mathcal{X}_{\bar{S}}} f(\mathbf{x}_S^*, \mathbf{x}_{\bar{S}}) p(\mathbf{x}_{\bar{S}} | \mathbf{x}_S = \mathbf{x}_S^*),$$

where  $\mathcal{X}_{\bar{S}}$  denotes the feature space of the feature vector  $\mathbf{x}_{\bar{S}}$  which contains  $L^{|\bar{S}|}$  unique feature combinations.<sup>6</sup> We need the conditional probability  $p(\mathbf{x}_{\bar{S}} | \mathbf{x}_S = \mathbf{x}_S^*)$  for each combination of  $\mathbf{x}_{\bar{S}} \in \mathcal{X}_{\bar{S}}$ . These can be written as  $p(\mathbf{x}_{\bar{S}} | \mathbf{x}_S) = p(\mathbf{x}_{\bar{S}}, \mathbf{x}_S) / p(\mathbf{x}_S)$ , and then evaluated at the desired  $\mathbf{x}_S^*$ . Since all feature combinations correspond to hyper-rectangular subspaces of Gaussian features, we can compute all joint probabilities exactly using the cut-offs  $v_1, \dots, v_{L+1}$ :

$$p(x_1 = l_1, \dots, x_M = l_M) = P(v_{l_1} < \tilde{x}_1 \leq v_{l_1+1}, \dots, v_{l_M} < \tilde{x}_M \leq v_{l_M+1}),$$

for  $l_j = 1, \dots, L$  and  $j = 1, \dots, M$ . Here  $p$  denotes the joint probability mass function of  $\mathbf{x}$  while  $P$  denotes the joint continuous distribution function of  $\tilde{\mathbf{x}}$ . The probability on the right-hand side is easily computed using the cumulative distribution function of the multivariate Gaussian distribution in the R-package `mvtnorm`. The marginal and joint probability functions based on only a subset of the features are computed analogously based on a subset of the full Gaussian distribution, which is also Gaussian.

## F Number of Monte Carlo Samples $K$

In this appendix, we illustrate that  $K = 250$  is a sufficient number of Monte Carlo samples in (3) for the continuous simulation studies in Section 4.2. In Table 1, we presented the average MAE when  $K = 250$ . In Table 7, we see that a larger value of  $K = 500$  or  $K = 1000$  marginally decrease the MAE in some experiments, but this comes at a larger computational cost. Thus, if time is not a limiting factor, we recommend to use a large value of  $K$ . In practice, with limited time to generate the estimated Shapley values, we find  $K = 250$  to be sufficient for

---

<sup>6</sup>Redelmeier et al. (2020) incorrectly write  $|\bar{S}|^L$ .

$N_{\text{train}}$	Method	$K = 500$				$K = 1000$			
		$\overline{\text{MAE}}$ for each $\kappa$				$\overline{\text{MAE}}$ for each $\kappa$			
		1	2	3	CPU	1	2	3	CPU
100	Independence	0.2694	0.1916	0.1630	0.41	0.2694	0.1916	0.1630	0.40
	Empirical	0.1633	0.1585	0.1661	0.43	0.1633	0.1585	0.1661	0.43
	Gaussian	0.1343	0.1002	0.0945	11.84	0.1343	0.1001	0.0944	13.40
	Copula	0.1290	0.1023	0.0964	22.38	0.1289	0.1021	0.0962	33.09
	Ctree	0.1867	0.1649	0.1495	10.26	0.1864	0.1648	0.1494	11.29
	VAEAC	<b>0.1148</b>	<b>0.0941</b>	<b>0.0892</b>	15.57	<b>0.1126</b>	<b>0.0985</b>	<b>0.0858</b>	30.02
1000	Independence	0.2730	0.2224	0.1840	3.22	0.2730	0.2224	0.1840	3.17
	Empirical	0.0890	0.0741	0.0751	3.67	0.0890	0.0741	0.0751	3.70
	Gaussian	0.1193	0.0786	0.0660	11.89	0.1194	0.0786	0.0658	13.30
	Copula	0.1085	0.0926	0.0764	23.00	0.1084	0.0924	0.0761	33.75
	Ctree	0.0894	0.0865	0.0812	11.55	0.0891	0.0864	0.0808	12.97
	VAEAC	<b>0.0674</b>	<b>0.0568</b>	<b>0.0525</b>	17.25	<b>0.0675</b>	<b>0.0547</b>	<b>0.0549</b>	31.58
5000	Independence	0.2759	0.2299	0.1950	4.60	0.2760	0.2298	0.1948	4.61
	Empirical	0.0742	0.0479	0.0450	5.13	0.0742	0.0479	0.0450	5.15
	Gaussian	0.1372	0.0788	0.0650	11.86	0.1373	0.0789	0.0648	13.28
	Copula	0.1067	0.0914	0.0773	25.37	0.1066	0.0911	0.0770	36.24
	Ctree	0.0541	0.0543	0.0538	19.78	0.0538	0.0540	0.0534	20.98
	VAEAC	<b>0.0478</b>	<b>0.0403</b>	<b>0.0406</b>	26.18	<b>0.0433</b>	<b>0.0399</b>	<b>0.0358</b>	40.31

**Table 7:** Same set up as in Table 1, that is,  $M = 10$ -dimensional  $\text{Burr}(\kappa)$  data with 20 repetitions, but with  $K = 500$  and  $K = 1000$  Monte Carlo samples. The **VAEAC** approach is the most accurate method in all experiments, but its sampling time has linearly increased with  $K$ .

this particular setting. We see that **VAEAC** is the best method in all 9 experiments when we increase the number of Monte Carlo samples. The training time of **VAEAC** is the same as before, as we have used the same hyperparameters, see Appendix C, but the sampling time increase proportionally with  $K$ . That is, if  $K$  doubles the sampling time also doubles while the training time remains fixed. This tendency is not seen in all of the other methods. For example, the **empirical** approach uses approximately the same CPU time for  $K = 500$  and  $K = 1000$ , indicating that the fitting process is the time consuming task while the sampling process is insignificant.

## References

- Aas, K., Jullum, M., and Løland, A. (2021). “Explaining individual predictions when features are dependent: More accurate approximations to Shapley values”. In: *Artificial Intelligence* vol. 298, p. 103502.
- Aas, K., Nagler, T., et al. (2021). “Explaining predictive models using Shapley values and non-parametric vine copulas”. In: *Dependence Modeling* vol. 9, no. 1, pp. 62–81.
- Adadi, A. and Berrada, M. (2018). “Peeking inside the black-box: a survey on explainable artificial intelligence (XAI)”. In: *IEEE access* vol. 6, pp. 52138–52160.
- Arellano-Valle, R. B., Branco, M. D., and Genton, M. G. (2006). “A unified view on skewed distributions arising from selections”. In: *Canadian Journal of Statistics* vol. 34, no. 4, pp. 581–601.

- Blei, D. M., Kucukelbir, A., and McAuliffe, J. D. (2017). “Variational inference: A review for statisticians”. In: *Journal of the American statistical Association* vol. 112, no. 518, pp. 859–877.
- Bowman, S. R. et al. (Aug. 2016). “Generating Sentences from a Continuous Space”. In: *Proceedings of The 20th SIGNLL Conference on Computational Natural Language Learning*. Berlin, Germany: Association for Computational Linguistics, pp. 10–21.
- Breiman, L. (2001). “Random forests”. In: *Machine learning* vol. 45, no. 1, pp. 5–32.
- Chen, H. et al. (2020). “True to the Model or True to the Data?” In: *arXiv preprint arXiv:2006.16234*.
- Chen, T. et al. (2015). “Xgboost: extreme gradient boosting”. In: *R package version 0.4-2* vol. 1, no. 4, pp. 1–4.
- Covert, I., Lundberg, S. M., and Lee, S.-I. (2020). “Understanding global feature contributions with additive importance measures”. In: *arXiv preprint arXiv:2004.00668*.
- Douglas, L. et al. (Dec. 2017). “A Universal Marginalizer for Amortized Inference in Generative Models”. In: *Proceedings of 31st Conference on Neural Information Processing Systems (NIPS 2017)*.
- European Commission (2016). “Regulation EU 2016/679 of the European Parliament and of the Council of 27 April 2016; General Data Protection Regulation”. In: *Official Journal of the European Union*.
- Frye, C. et al. (2021). “Shapley explainability on the data manifold”. In: *International Conference on Learning Representations*.
- Fryer, D., Strümke, I., and Nguyen, H. (2021). “Shapley values for feature selection: The good, the bad, and the axioms”. In: *ArXiv* vol. abs/2102.10936.
- Gautam, D. et al. (2020). “Masking schemes for universal marginalisers”. In: *CoRR* vol. abs/2001.05895. arXiv: 2001.05895.
- Genz, A. and Bretz, F. (2009). *Computation of multivariate normal and t probabilities*. Vol. 195. Springer Science & Business Media.
- Giudici, P. and Raffinetti, E. (2021). “Shapley-Lorenz eXplainable artificial intelligence”. In: *Expert Systems with Applications* vol. 167, p. 114104.
- Goodfellow, I., Bengio, Y., and Courville, A. (2016). *Deep Learning*. MIT Press.
- Goodfellow, I., Pouget-Abadie, J., et al. (2014). “Generative adversarial nets”. In: *Advances in neural information processing systems* vol. 27.
- Gurney, K. (2018). *An introduction to neural networks*. CRC press.
- Hart, S. (1989). “Shapley value”. In: *Game Theory*. Springer, pp. 210–216.
- Hothorn, T., Hornik, K., and Zeileis, A. (2006). “Unbiased recursive partitioning: A conditional inference framework”. In: *Journal of Computational and Graphical statistics* vol. 15, no. 3, pp. 651–674.
- Ivanov, O., Figurnov, M., and Vetrov, D. (2019). “Variational Autoencoder with Arbitrary Conditioning”. In: *International Conference on Learning Representations*.
- Joe, H. (1996). “Families of m-variate distributions with given margins and  $m(m-1)/2$  bivariate dependence parameters”. In: *Lecture Notes-Monograph Series*, pp. 120–141.
- Jullum, M., Løland, A., et al. (2020). “Detecting money laundering transactions with machine learning”. In: *Journal of Money Laundering Control*.
- Jullum, M., Redelmeier, A., and Aas, K. (2021). *groupShapley: Efficient prediction explanation with Shapley values for feature groups*. arXiv: 2106.12228 [stat.ML].
- Karras, T. et al. (2020). “Analyzing and improving the image quality of stylegan”. In: *Proceedings of the IEEE/CVF Conference on Computer Vision and Pattern Recognition*, pp. 8110–8119.

- Kingma, D. P. and Ba, J. (2015). “Adam: A Method for Stochastic Optimization”. In: *3rd International Conference on Learning Representations, ICLR 2015, San Diego, CA, USA, May 7-9, 2015, Conference Track Proceedings*. Ed. by Bengio, Y. and LeCun, Y.
- Kingma, D. P. and Welling, M. (2019). “An Introduction to Variational Autoencoders”. In: *Found. Trends Mach. Learn.* vol. 12, pp. 307–392.
- Kingma, D. P. and Welling, M. (2014). “Auto-Encoding Variational Bayes”. In: *2nd International Conference on Learning Representations, ICLR 2014, Banff, AB, Canada, April 14-16, 2014, Conference Track Proceedings*.
- Kourou, K. et al. (2015). “Machine learning applications in cancer prognosis and prediction”. In: *Computational and structural biotechnology journal* vol. 13, pp. 8–17.
- Kvamme, H. et al. (2018). “Predicting mortgage default using convolutional neural networks”. In: *Expert Systems with Applications* vol. 102, pp. 207–217.
- Lundberg, S. M., Erion, G. G., and Lee, S.-I. (2018). “Consistent individualized feature attribution for tree ensembles”. In: *arXiv preprint arXiv:1802.03888*.
- Lundberg, S. M. and Lee, S.-I. (2017). “A unified approach to interpreting model predictions”. In: *Advances in neural information processing systems*, pp. 4765–4774.
- Mao, X., Shen, C., and Yang, Y.-B. (2016). “Image restoration using very deep convolutional encoder-decoder networks with symmetric skip connections”. In: *Advances in neural information processing systems* vol. 29, pp. 2802–2810.
- Merrick, L. and Taly, A. (2020). “The Explanation Game: Explaining Machine Learning Models Using Shapley Values”. In: *Machine Learning and Knowledge Extraction*. Lecture Notes in Computer Science. Cham: Springer International Publishing, pp. 17–38.
- Mohammed, G. R. et al. (2020). “Predicting the Age of Abalone from Physical Measurements Using Artificial Neural Network”. In: *International Journal of Academic and Applied Research (IJAAR)* vol. 4, no. 11.
- Molnar, C. (2019). *Interpretable Machine Learning. A Guide for Making Black Box Models Explainable*. lulu.com.
- Mustafa, M. et al. (2019). “CosmoGAN: creating high-fidelity weak lensing convergence maps using Generative Adversarial Networks”. In: *Computational Astrophysics and Cosmology* vol. 6, no. 1, p. 1.
- Nash, W. J. et al. (1994). “The population biology of Abalone (*Haliotis* species) in Tasmania. I. Blacklip Abalone (*H. rubra*) from the North Coast and Islands of Bass Strait.” In: *Sea Fisheries Division, Technical Report* vol. 48, p411.
- Owen, A. B. (2014). “Sobol’ indices and Shapley value”. In: *SIAM/ASA Journal on Uncertainty Quantification* vol. 2, no. 1, pp. 245–251.
- Paszke, A. et al. (2019). “Pytorch: An imperative style, high-performance deep learning library”. In: *Advances in neural information processing systems* vol. 32, pp. 8026–8037.
- Potdar, K., Pardawala, T. S., and Pai, C. D. (2017). “A comparative study of categorical variable encoding techniques for neural network classifiers”. In: *International journal of computer applications* vol. 175, no. 4, pp. 7–9.
- Python Core Team (2020). *Python: A dynamic, open source programming language*. Python Software Foundation.
- R Core Team (2020). *R: A Language and Environment for Statistical Computing*. R Foundation for Statistical Computing. Vienna, Austria.
- Redelmeier, A., Jullum, M., and Aas, K. (2020). “Explaining predictive models with mixed features using Shapley values and conditional inference trees”. In: *International Cross-Domain Conference for Machine Learning and Knowledge Extraction*. Springer, pp. 117–137.

- Rezende, D. J., Mohamed, S., and Wierstra, D. (2014). “Stochastic backpropagation and approximate inference in deep generative models”. In: *International conference on machine learning*. PMLR, pp. 1278–1286.
- Roberts, A. et al. (2018). “A hierarchical latent vector model for learning long-term structure in music”. In: *International conference on machine learning*. PMLR, pp. 4364–4373.
- Ronneberger, O., Fischer, P., and Brox, T. (2015). “U-net: Convolutional networks for biomedical image segmentation”. In: *International Conference on Medical image computing and computer-assisted intervention*. Springer, pp. 234–241.
- Roth, A. E. (1988). *The Shapley value: essays in honor of Lloyd S. Shapley*. Cambridge University Press.
- Sahin, E. et al. (2018). “Abalone life phase classification with deep learning”. In: *2018 5th International Conference on Soft Computing & Machine Intelligence (ISCMI)*. IEEE, pp. 163–167.
- Sellereite, N. and Jullum, M. (2019). “shapr: An R-package for explaining machine learning models with dependence-aware Shapley values”. In: *Journal of Open Source Software* vol. 5, no. 46, p. 2027.
- Shapley, L. S. (1953). “A value for n-person games”. In: *Contributions to the Theory of Games* vol. 2, no. 28, pp. 307–317.
- Simon, I. et al. (2018). *Learning a Latent Space of Multitrack Measures*. arXiv: 1806.00195 [stat.ML].
- Smith, J. S., Wu, B., and Wilamowski, B. M. (2018). “Neural network training with Levenberg–Marquardt and adaptable weight compression”. In: *IEEE transactions on neural networks and learning systems* vol. 30, no. 2, pp. 580–587.
- Sohn, K., Lee, H., and Yan, X. (2015). “Learning structured output representation using deep conditional generative models”. In: *Advances in neural information processing systems* vol. 28, pp. 3483–3491.
- Strumbelj, E. and Kononenko, I. (2010). “An efficient explanation of individual classifications using game theory”. In: *The Journal of Machine Learning Research* vol. 11, pp. 1–18.
- (2014). “Explaining prediction models and individual predictions with feature contributions”. In: *Knowledge and information systems* vol. 41, no. 3, pp. 647–665.
- Takahasi, K. (1965). “Note on the multivariate burr’s distribution”. In: *Annals of the Institute of Statistical Mathematics* vol. 17, no. 1, pp. 257–260.
- Ushey, K., Allaire, J., and Tang, Y. (2020). *reticulate: Interface to ‘Python’*. R package version 1.18.
- Wright, M. N. and Ziegler, A. (2017). “ranger: A Fast Implementation of Random Forests for High Dimensional Data in C++ and R”. In: *Journal of Statistical Software* vol. 77, no. 1, pp. 1–17.
- Yari, G. and Jafari, A. M. (2006). “Information and Covariance Matrices for Multivariate Pareto (IV), Burr, and Related Distributions”. In: *International Journal of Industrial Engineering & Production Research* vol. 17, pp. 61–69.
- Yoon, J., Jordon, J., and Schaar, M. (2018). “Gain: Missing data imputation using generative adversarial nets”. In: *International Conference on Machine Learning*. PMLR, pp. 5689–5698.